

Fluid Cohomology

HANG YIN, University of California, San Diego

MOHAMMAD SINA NABIZADEH, University of California, San Diego

BAICHUAN WU, University of California, San Diego

STEPHANIE WANG, University of California, San Diego

ALBERT CHERN, University of California, San Diego

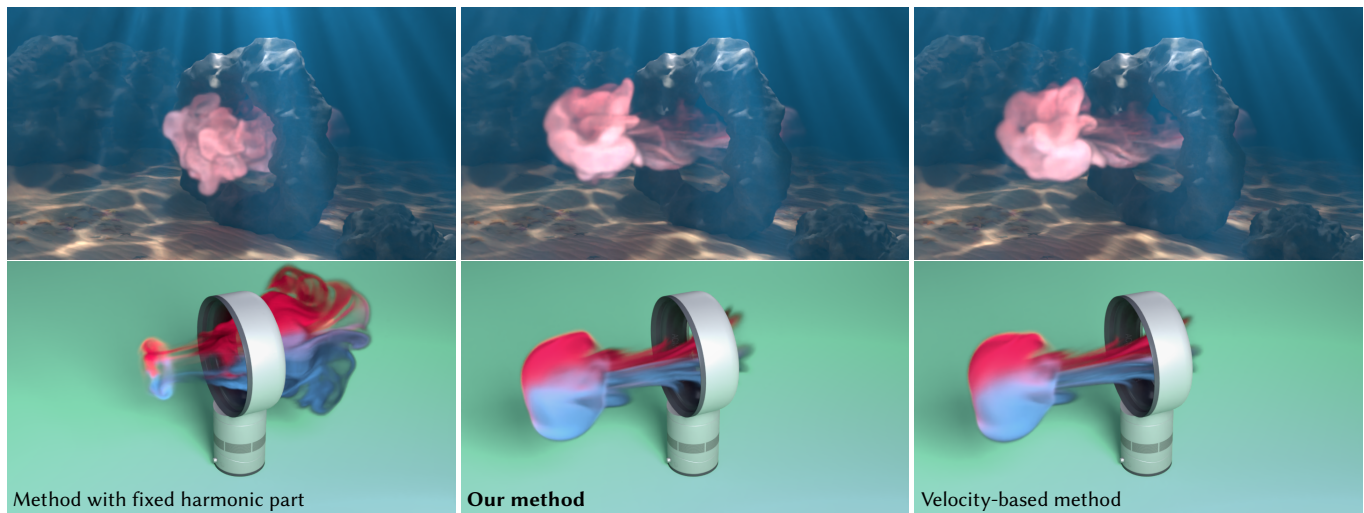


Fig. 1. With torus-shaped obstacles in the fluid domain, the cohomology of the fluid velocity becomes nontrivial. By incorporating the correct time-evolution of the harmonic parts, our method (middle) removes the unphysical behaviors of a general vorticity-streamfunction method (left). We compare our result against ground truth which is produced by a velocity-based method using pressure projection (right).

The *vorticity-streamfunction* formulation for incompressible inviscid fluids is the basis for many fluid simulation methods in computer graphics, including vortex methods, streamfunction solvers, spectral methods, and Monte Carlo methods. We point out that current setups in the vorticity-streamfunction formulation are insufficient at simulating fluids on general non-simply-connected domains. This issue is critical in practice, as obstacles, periodic boundaries, and nonzero genus can all make the fluid domain multiply connected. These scenarios introduce nontrivial cohomology components to the flow in the form of harmonic fields. The dynamics of these harmonic fields have been previously overlooked. In this paper, we derive the missing equations of motion for the fluid cohomology components. We elucidate the physical laws associated with the new equations, and show their importance in reproducing physically correct behaviors of fluid flows on domains with general topology.

Authors' addresses: Hang Yin, University of California, San Diego, h7yin@ucsd.edu; Mohammad Sina Nabizadeh, University of California, San Diego, mnabizad@ucsd.edu; Baichuan Wu, University of California, San Diego, bwu@ucsd.edu; Stephanie Wang, University of California, San Diego; Albert Chern, University of California, San Diego, alchern@ucsd.edu.

Permission to make digital or hard copies of part or all of this work for personal or classroom use is granted without fee provided that copies are not made or distributed for profit or commercial advantage and that copies bear this notice and the full citation on the first page. Copyrights for third-party components of this work must be honored. For all other uses, contact the owner/author(s).

© 2023 Copyright held by the owner/author(s).

0730-0301/2023/8-ART1

<https://doi.org/10.1145/3592402>

CCS Concepts: • **Computing methodologies** → **Physical simulation**; • **Mathematics of computing** → **Algebraic topology**; *Partial differential equations*; • **Applied computing** → *Physics*.

Additional Key Words and Phrases: Fluid dynamics, homology theory

ACM Reference Format:

Hang Yin, Mohammad Sina Nabizadeh, Baichuan Wu, Stephanie Wang, and Albert Chern. 2023. Fluid Cohomology. *ACM Trans. Graph.* 42, 4, Article 1 (August 2023), 24 pages. <https://doi.org/10.1145/3592402>

1 INTRODUCTION

One of the main tasks in fluid simulation in computer graphics is to approximate the solutions to the *incompressible Euler equations* which govern the dynamics of the velocity fields of incompressible inviscid fluids. One approach is to instead simulate the equations in the *vorticity-streamfunction* formulation of fluid dynamics. This formulation takes the *vorticity field* as the primary variable, whereas the velocity field is reconstructed from the vorticity through a streamfunction [Bridson 2015, §14.2; Chorin and Marsden 1990, §1.2]. Numerical methods based on this formulation have more direct controls over the preservation of local vorticity. The velocity fields derived from the streamfunction are automatically divergence free. Researchers have adopted this formulation to simulate vortex dynamics [Gamito et al. 1995; Elcott et al. 2007; Zhang et al. 2015] and two-phase flows [Ando et al. 2015a]. Other usage of the



Fig. 2. Fluid simulation on minimal surfaces plays an important role in texturing soap films. Costa’s surface is a minimal surface with genus one and three boundaries, and therefore nontrivial cohomology. Our method is the first vorticity-streamfunction method to correctly simulate fluid on generic surfaces including those with complicated topology.

vorticity-streamfunction formulation in fluid simulation includes [De Witt et al. 2012] (a vorticity-based spectral method) and [Rioux-Lavoie et al. 2022] (a Monte Carlo method). Vorticity-streamfunction formulation is especially advantageous for fluids on 2D domains including curved surfaces, as the vorticity equation requires only a scalar advection, as opposed to a vector advection in velocity-based solvers [Yaeger et al. 1986; Elcott et al. 2007; Azencot et al. 2014]. The use of streamfunctions is also the foundation for divergence-free flow syntheses [Bridson et al. 2007; Sato et al. 2014, 2021] and interpolations [Chang et al. 2019, 2022].

While vorticity-streamfunction formulation is well established, the equations therein are insufficient at describing fluid flows on general domains, in particular, those that are non-simply-connected. Such scenarios with nontrivial topology are common, as multiply-connectedness can arise from the presence of obstacles (Fig. 1), periodic boundary conditions, or the domain being a surface¹ with nonzero genus (Fig. 2). The issue with multiply-connected domains is that they support irrotational flows, known as *harmonic fields*, that cannot be represented by the vorticity variable. In topological terms, the harmonic fields represent the *1st de Rham cohomology* components of the flow.² A rarely discussed fact is that *harmonic parts have their own dynamics*. The vorticity equation alone is not enough to describe an Euler fluid flow. One must consider a coupled system between the vorticity and the harmonic components.

Previous Approaches. Previous work fills in the harmonic components using various treatments during the recovery of the velocity from the vorticity variable. One approach is to reconstruct the velocity field from the vorticity data using the Biot–Savart integral (which works in the entire Euclidean space with no obstacles) followed by adding a pressure gradient [Lin 1941; Bridson 2015, §14.3.7; Weißmann and Pinkall 2012; Ishida et al. 2022], a vortex sheet over the obstacle surface [Park and Kim 2005; Weißmann and Pinkall 2010; Golas et al. 2012; Brochu et al. 2012; Vines et al. 2013; Zhang

¹Fluid dynamics on general surfaces especially attracts attention in computer graphics [Stam 2003; Shi and Yu 2004; Azencot et al. 2014; Huang et al. 2020; Ishida et al. 2020; Cui et al. 2021], geometry [Boatto and Koiller 2015; Padilla 2018] and biophysics [Rank and Voigt 2021]. See references within for surveys of the topic.

²In calculus terms, the de Rham cohomology describes the difference between a curl-free vector field and the gradient of a function, and between a divergence-free field and the curl of a vector potential.

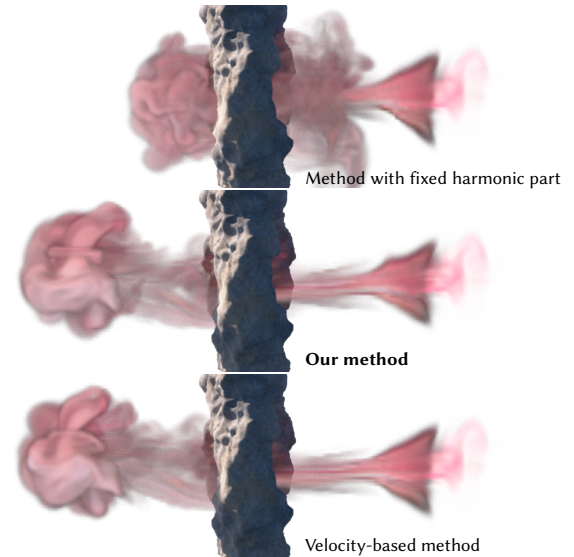


Fig. 3. Side-view of smoke passing through a torus-shaped obstacle. Also see the top row of Fig. 1 (see video 00:31).

and Bridson 2014; Xiong et al. 2021], or mirror-reflected vortices in the obstacles of specific shapes (e.g. a plane [Angelidis and Neyret 2005]) to prevent the velocity from penetrating the obstacles. These methods do ensure correct dynamics of the harmonic components implicitly. However, they work only when the fluid domain is a subset of a Euclidean space and when the circulation around every handle of the obstacle is zero. In particular, it does not apply to flows on surfaces, on periodic domains, or with nonzero circulations around obstacles.

A few methods skip the vorticity variable and directly reconstruct streamfunctions from the velocity data on a grid. This technique is intended to obtain the exact divergence-free flow interpolation facilitated by the streamfunction [Biswas et al. 2016; Chang et al. 2022]. Unlike integrating from vorticity, the construction is by path-integrating velocity, which will not lose the harmonic information of the velocity. However, as we show in our paper (Proposition 5), global streamfunctions exist only for special cases (e.g. when the multiply-connectedness arises from removing obstacles from a simply-connected domain).³

Another approach is to encapsulate the degrees of freedom of harmonic fields into inhomogeneous boundary conditions for the streamfunctions [Mizukami 1983]. Determining the boundary conditions for the streamfunction on each “island” is a well-known problem in oceanography [Godfrey 1989; Pedlosky et al. 1997]. This is commonly known as the *island rule*, which boils down to solving a global Dirichlet-to-Neumann map problem. Unfortunately, the treatment only resolves harmonic fields that arise from obstacles in 2D. The analogous formulations in 3D are more sophisticated as they involve keeping track of circulations along flowing loops. In general, the approach cannot account for harmonic fields arising

³These methods are still useful for constructing local streamfunctions.

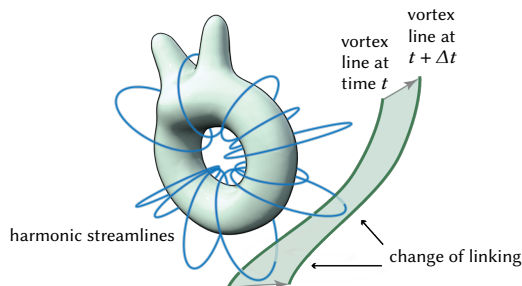


Fig. 4. The change of linking between harmonic streamlines (blue) and fluid vortex lines (green) in a fluid domain exterior to the obstacle (torus).

from periodic boundary conditions or nonzero genus of a surface domain.

Lastly, a commonly adopted method accounting for harmonic fields is to extract the harmonic component of the initial velocity and add it to the streamfunction-represented velocity at each future time step [Elcott et al. 2007, §4.5; Azencot et al. 2014, Eq. (1); Ando et al. 2015a, §3]. This method keeps the harmonic parts *fixed*, as if they were constant in time. If the initial harmonic components are all zero, then the treatment is equivalent to neglecting harmonic components on closed surfaces [Boatto and Koiller 2015, §3], or setting a (tangentially) zero boundary condition on the streamfunctions [Gamito et al. 1995; Rioux-Lavoie et al. 2022, §4.1]. While most of these approaches address the nontrivial cohomology generated by both the obstacles and the genus, they ignore the dynamics of the harmonic parts. While it might seem that Kelvin’s circulation theorem would imply the conservation of harmonic parts over time, this is in fact a misinterpretation of the theorem and a misgeneralization of the preservation of harmonic fields when there is no vorticity [Thomson 1868]. The absence of changes in harmonic parts can lead to unrealistic fluid behaviors. For example, omitting the harmonic dynamics will lead to a fixed total flux over every cross-section of the domain, e.g. the cross-section of the tunnel in Fig. 1. Notably, a jet flow shot through the tunnel will be obstructed and disrupted by an artificial zero total flux condition persisting since the initial condition. Similar anomalies are pointed out in [Rioux-Lavoie et al. 2022, pp 12] and an errata [Ando et al. 2015b].

New Formulation. In this paper, we derive the missing dynamics of the harmonic parts for the vorticity-streamfunction formulation of the Euler equations. The system applies to all multiply-connected fluid domains. The dynamics are presented in a simple form that is easy to incorporate into previous vorticity-streamfunction methods. The dynamics can be summarized as a new physical law of Euler fluids:

For each cohomology component associated with a cross-section of the domain, the difference between the *fluid cross-sectional flux* and the *total linking number* (or *winding number* in 2D) between the *harmonic field streamlines* and the *fluid vortex lines* (or *vortex points* in 2D) is a constant of motion (see Fig. 4).

In other words, the harmonic components, which are all directly related to the cross-sectional fluxes, evolve precisely at the rate at

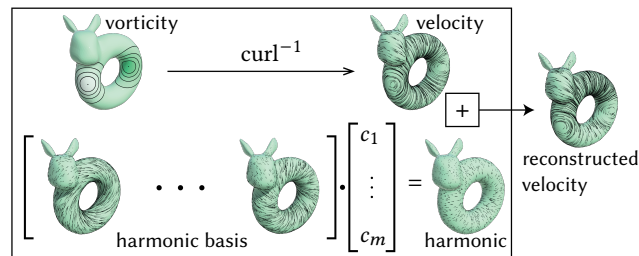


Fig. 5. Our pipeline of reconstructing the velocity field from both the advected vorticity and the correctly updated harmonic coefficients (c_1, \dots, c_m) .

which a vortex line cuts through a harmonic streamline. Moreover, this seemingly intricate rate of topological changes boils down to a simple integral formula $\int_M (\mathbf{u} \times \mathbf{w}) \cdot \mathbf{h}_i dx$ in terms of the computationally available velocity \mathbf{u} , vorticity \mathbf{w} and harmonic basis \mathbf{h}_i , which makes incorporating the new dynamics light-weight and highly practical. This is the same as the time-evolution of coefficients of a vector spectral basis, which includes the harmonic basis, as proposed in the velocity-based model reduction work by [Liu et al. 2015]. We point out that this equation for the harmonic basis is necessary to account for the missing dynamics of the harmonic components in the vorticity-streamfunction formulation, making the formulation suitable for fluid simulations on all general domains. We also describe our new conservation law from the perspective of Hamiltonian fluid mechanics as a *Casimir invariant*. Note that the only previously known nontrivial example of a Casimir invariant for 3D incompressible fluids is the *helicity* [Khesin et al. 2022], which has played important roles in meteorology, topological fluid mechanics, and plasma physics. The discovery of the new Casimir invariant will facilitate more exciting studies in these areas.

In practice, incorporating the new evolution equation of the harmonic components is quite simple. Express the fluid velocity field $\mathbf{u} = \text{curl}^{-1} \mathbf{w} + \sum_i c_i \mathbf{h}_i$ in terms of the vorticity field \mathbf{w} and an orthonormal basis $(\mathbf{h}_i)_i$ for the harmonic fields (see Fig. 5). On top of a traditional vorticity equation solver that updates \mathbf{w} , one only needs to add an extra step for updating the coefficients $\dot{c}_i = \int_M (\mathbf{u} \times \mathbf{w}) \cdot \mathbf{h}_i dx$ (see Fig. 6). Through numerical examples, we show the importance of the dynamics of the harmonic components for reproducing physically correct behaviors of fluid flows on surfaces and on 3D domains with nontrivial topology (Fig. 3).

Contributions. Highlights of this paper include

- Deriving the missing dynamics of the harmonic parts for incompressible inviscid fluids, and a simple and practical method for incorporating it to both 2D and 3D simulations (Section 4).
- A new conservation law between harmonic streamlines and vortex lines in an Euler fluid (Theorem 2).
- The first vorticity-streamfunction-based fluid solver on general surfaces that is consistent with the Euler equations. (Alg. 2 (Fig. 2)).
- A new Hamiltonian formulation for incompressible Euler equations featuring new Casimir invariants (Section 6).

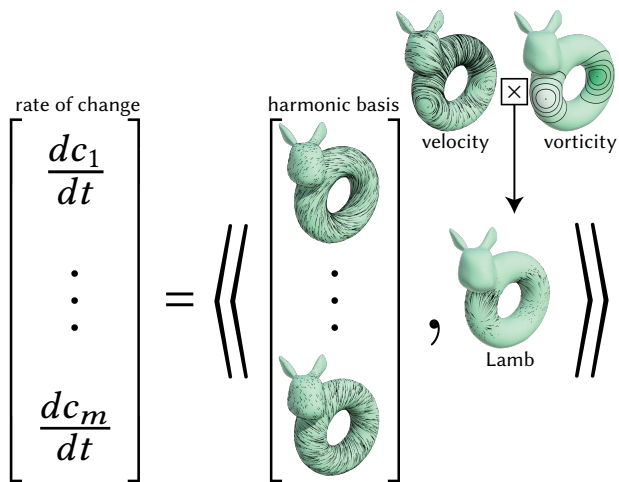


Fig. 6. The rate of change of the harmonic coefficients ($dc_1/dt, \dots, dc_m/dt$) is computed by projecting the Lamb vector onto the harmonic basis. The Lamb vector is the cross-product of velocity and vorticity fields.

1.1 Additional Related Work

In addition to computer graphics and oceanography, we briefly review the fundamental research on the vorticity-streamfunction formulation in related areas.

1.1.1 Computational Fluid Dynamics. The vorticity-streamfunction formulation is also extensively studied in the literature of computational fluid dynamics (CFD). There, the majority of attention is drawn to finding a compatible boundary condition in the presence of viscosity. Under viscosity, the boundary value of vorticity diffuses to the interior and can influence the resulting streamfunction from the Poisson solve. Therefore, the question becomes how to couple the boundary values of the vorticity and the streamfunction such that the resulting velocity satisfies both the no-through and no-slip conditions at the boundary. An initial pursuit for the boundary treatments by [Thom 1933] is followed by many variants [Taylor and Hood 1973; Orszag and Israeli 1974], revisions, and discussions [Quartapelle and Valz-Gris 1981; Anderson 1989; Quartapelle 1993; E and Liu 1996] throughout the remainder of the century. A comprehensive review on the highly debated topic of boundary conditions for the vorticity-streamfunction formulation can be found in [Rempfer 2006, §3.4]. However, despite the large body of work searching for a proper vorticity-streamfunction formulation in CFD, few mentioned the effect of non-trivial topology. Different cohomology data of the flow can correspond to different sets of coupled vorticity-streamfunction boundary configurations, but these cohomological factors, which have their own dynamics, are irrotational and invisible to the vorticity variable. A few vorticity-streamfunction formulations that properly handle the cases of non-simply-connected domains are described in [Mizukami 1983; Tezduyar et al. 1988]. However, these approaches only account for the non-simply-connectedness induced from obstacles rather than for general cases where cohomology components can arise.

1.1.2 Geometric Fluid Dynamics. Geometric fluid dynamics is the mathematical discipline that discusses fluid dynamics in the geometric mechanics framework, including Hamiltonian systems [Salmon 1988; Morrison 1998] and geodesic equations on Lie groups [Arnold 1966]. The mathematical foundation has inspired many structure-preserving fluid simulation algorithms in computer graphics [Elcott et al. 2007; Pavlov et al. 2011; Azencot et al. 2014; Liu et al. 2015; Chern et al. 2016; Yang et al. 2021; Nabizadeh et al. 2022]. There, the Hamiltonian formulation of fluid dynamics often employs the vorticity-streamfunction formulation [Marsden and Weinstein 1983; Morrison 1998]. Precisely, the phase space (with Poisson structure) is given by the space of vorticities, and the evaluation of Hamiltonian is defined with the aid of streamfunctions. Unfortunately, these descriptions would omit the cohomology components of the velocity. A way to take cohomology components into account is to define the phase space as the quotient space $\Omega^1/d\Omega^0$ of velocity covectors modulo exact forms [Arnold and Khesin 1998, Theorem I.7.5; Osledeets 1989; Pavlov et al. 2011; Nabizadeh et al. 2022]. However, this approach makes the phase space more abstract than the physically more understandable vorticity. To our knowledge, our work is the first to express the Hamiltonian formulation explicitly in terms of both the vorticity and the cross-sectional fluxes that parameterize the cohomology. Under this coordinate, we discover new *Casimir invariants* [Morrison 1998; Khesin and Chekanov 1989] that relate the cohomological flux and its linking number with the vortex lines.

A line of work that examines fluids' cohomology is the study of the *commutant* of the Lie group of volume-preserving diffeomorphisms [Arnold 1969; Banyaga 1978; Arnold and Khesin 1998, Definition I.7.12]. They give an insightful characterization of the subgroup of flow maps generated by velocities that have no harmonic parts. This subgroup turns out to be the commutant of the group of all flow maps. However, the line of work did not comment on whether the physical fluid flow would stay or leave this commutant subgroup. The recent results on the *helicity uniqueness conjecture* [Khesin et al. 2022] were also restricted to this subgroup. Our work includes illustrative examples that show a fluid flow with initially zero harmonic components will later gain harmonic components. We show that fluid flows are generally not constrained in the commutant subgroup of the Lie group of volume-preserving flow maps.

2 BACKGROUND

In this section, we review the vorticity-streamfunction formulation for incompressible fluids. We present the theory of the paper in exterior calculus for its ability to unify 2D and 3D languages and to provide geometric intuitions. Readers who are less familiar with exterior calculus may find the following resources useful: (a) a comprehensive review of exterior calculus in Appendix A.1, (b) translations of exterior calculus operations to vector calculus in Tables 1 and 2, and (c) a summary of this section written in terms of vector calculus in Section 2.6.

We use the standard notations [Lee 2013, Chapter 17; Hatcher 2002, Chapter 2] of $C_\bullet(M)$, $Z_\bullet(M)$, $B_\bullet(M)$, $H_\bullet(M)$ to denote, respectively, the space of chains, cycles, boundaries, and homologies, and

Table 1. Exterior calculus operations written in terms of vector calculus operations on a 2D domain M . Here, a, b are scalar functions, $\mathbf{a}, \mathbf{b}, \mathbf{v}$ are vector fields, and \mathcal{J} is the 90° rotation operator. The map $j: \partial M \hookrightarrow M$ is the inclusion map of the boundary, whose normal vector is denoted by \mathbf{n} .

	$\alpha = a \in \Omega^0$	$\alpha = \mathbf{a}^b \in \Omega^1$	$\alpha = \star \mathbf{a} \in \Omega^2$	Meaning
$d\alpha$	$(\nabla \mathbf{a})^b$	$\star \left(\frac{\partial a_2}{\partial x_1} - \frac{\partial a_1}{\partial x_2} \right)$	0	Exterior derivative
$\delta\alpha$	0	$-\nabla \cdot \mathbf{a}$	$(-\mathcal{J}\nabla \mathbf{a})^b$	Codifferential
$i_{\mathbf{v}}\alpha$	0	$\mathbf{v} \cdot \mathbf{a}$	$(\mathbf{a}\mathcal{J}\mathbf{v})^b$	Interior product
$\alpha \wedge b$	ab	$(ba)^b$	$\star(ab)$	Wedge product
$\alpha \wedge \mathbf{b}^b$	$(ab)^b$	$\star(a_1b_2 - a_2b_1)$	0	
$\alpha \wedge (\star \mathbf{b}^b)$	$(\mathbf{a}\mathcal{J}\mathbf{b})^b$	$\star(\mathbf{a} \cdot \mathbf{b})$	0	
$\alpha \wedge (\star b)$	$\star(ab)$	0	0	
$\mathcal{L}_{\mathbf{v}}\alpha$	$\mathbf{v} \cdot \nabla a$	$\left(\mathbf{v} \cdot \nabla \mathbf{a} + (\nabla \mathbf{v})^T \mathbf{a} \right)^b$	$\star \left(\mathbf{v} \cdot \nabla \mathbf{a} + (\nabla \cdot \mathbf{v}) \mathbf{a} \right)$	Lie derivative
$j^*\alpha = 0$	$a _{\partial M} = 0$	$\mathbf{a} _{\partial M} \parallel \mathbf{n}$		Dirichlet BC
$j^*\star\alpha = 0$		$\mathbf{a} _{\partial M} \perp \mathbf{n}$	$a _{\partial M} = 0$	Co-Dirichlet BC

Table 2. Same as Table 1 but on a 3D domain.

	$\alpha = a \in \Omega^0$	$\alpha = \mathbf{a}^b \in \Omega^1$	$\alpha = \star \mathbf{a}^b \in \Omega^2$	$\alpha = \star \mathbf{a} \in \Omega^3$
$d\alpha$	$(\nabla \mathbf{a})^b$	$\star(\nabla \times \mathbf{a})^b$	$\star(\nabla \cdot \mathbf{a})$	0
$\delta\alpha$	0	$-\nabla \cdot \mathbf{a}$	$(\nabla \times \mathbf{a})^b$	$\star(-\nabla \mathbf{a})^b$
$i_{\mathbf{v}}\alpha$	0	$\mathbf{v} \cdot \mathbf{a}$	$(-\mathbf{v} \times \mathbf{a})^b$	$\star(\mathbf{a}\mathbf{v})^b$
$\alpha \wedge b$	ab	$(ba)^b$	$\star(ba)^b$	$\star(ab)$
$\alpha \wedge \mathbf{b}^b$	$(ab)^b$	$\star(\mathbf{a} \times \mathbf{b})^b$	$\star(\mathbf{a} \cdot \mathbf{b})$	0
$\alpha \wedge (\star \mathbf{b}^b)$	$\star(ab)^b$	$\star(\mathbf{a} \cdot \mathbf{b})$	0	0
$\alpha \wedge (\star b)$	$\star(ab)$	0	0	0
$\mathcal{L}_{\mathbf{v}}\alpha$	$\mathbf{v} \cdot \nabla a$	$\left(\mathbf{v} \cdot \nabla \mathbf{a} + (\nabla \mathbf{v})^T \mathbf{a} \right)^b$	$\star \left(\mathbf{v} \cdot \nabla \mathbf{a} - \mathbf{a} \cdot \nabla \mathbf{v} + (\nabla \cdot \mathbf{v}) \mathbf{a} \right)^b$	$\star \left(\mathbf{v} \cdot \nabla \mathbf{a} + (\nabla \cdot \mathbf{v}) \mathbf{a} \right)$
$j^*\alpha = 0$	$a _{\partial M} = 0$	$\mathbf{a} _{\partial M} \parallel \mathbf{n}$	$\mathbf{a} _{\partial M} \perp \mathbf{n}$	
$j^*\star\alpha = 0$		$\mathbf{a} _{\partial M} \perp \mathbf{n}$	$\mathbf{a} _{\partial M} \parallel \mathbf{n}$	$a _{\partial M} = 0$

$C_{\bullet}(M, \partial M)$, $Z_{\bullet}(M, \partial M)$, $B_{\bullet}(M, \partial M)$, $H_{\bullet}(M, \partial M)$ for their relative-to-boundary counterparts. See Appendix A.2 for further discussion on homology and relative homology.

2.1 Euler Equations

The incompressible inviscid fluid is governed by the following *Euler equations*. We assume the fluid density to be 1. On an n -dimensional fluid domain M ($n = 2$ or 3), the time-dependent fluid velocity vector field $\mathbf{u} \in \Gamma(TM)$ evolves under

$$\begin{cases} \frac{\partial}{\partial t} \mathbf{u} + \mathbf{u} \cdot \nabla \mathbf{u} = -\nabla p & \text{in } M; \text{ (momentum equation),} & (1a) \\ \nabla \cdot \mathbf{u} = 0 & \text{in } M; \text{ (divergence-free),} & (1b) \\ \mathbf{u} \cdot \mathbf{n} = 0 & \text{on } \partial M; \text{ (no-through boundary).} & (1c) \end{cases}$$

Here, \mathbf{n} denotes the normal vector of the domain boundary ∂M , and the scalar function $p \in \Omega^0(M)$ is the fluid pressure field. The covector (1-form) formulation [Nabizadeh et al. 2022] of (1) for the *velocity 1-form* $\eta = \mathbf{u}^b \in \Omega^1(M)$ is given by

$$\begin{cases} \frac{\partial}{\partial t} \eta + \mathcal{L}_{\mathbf{u}} \eta = -dp_L & \text{in } M; \text{ (circulation equation),} & (2a) \\ \delta \eta = 0 & \text{in } M; \text{ (co-closedness),} & (2b) \\ j^* \star \eta = 0 & \text{on } \partial M; \text{ (co-Dirichlet BC),} & (2c) \end{cases}$$

where d is the exterior derivative, δ the codifferential, $\mathcal{L}_{\mathbf{u}}$ the Lie derivative along $\mathbf{u} = \mathbf{u}^{\sharp}$, and \star the Hodge star. The *Lagrangian*

pressure $p_L \in \Omega^0(M)$ is related to physical pressure by $p_L = p - \frac{1}{2}|\mathbf{u}|^2$. The boundary condition is described using the pullback operator j^* of the canonical inclusion map $j: \partial M \hookrightarrow M$. Note that we call a differential form *Dirichlet* if it lies in $\ker(j^*)$, and *co-Dirichlet* if it lies in $\ker(j^*\star)$.⁴

All possible velocity fields form a linear subspace \mathcal{V}^1 of all the co-closed (2b) and co-Dirichlet (2c) 1-forms.

Definition 1 (Co-Dirichlet co-closed subspace). *Let the subspace of co-Dirichlet co-closed k -forms be denoted by*

$$\mathcal{V}^k := \left\{ \eta \in \Omega^k(M) \mid \delta \eta = 0, j^* \star \eta = 0 \right\} \subset \Omega^k(M). \quad (3)$$

The readers may verify that the co-Dirichlet co-closed subspace \mathcal{V}^k is L^2 -perpendicular⁵ to the space $\text{im}(d)$ of exact forms. Furthermore, together they span the space $\Omega^k(M)$ of all k -forms.

Proposition 1. $\Omega^k(M) = \text{im}(d) \oplus^{\perp} \mathcal{V}^k$.

PROOF. See Appendix E.1. \square

As a result of this proposition, one can view the Lagrangian pressure term dp_L in (2a) as the L^2 normal projection onto \mathcal{V}^1 . Note that by Stokes theorem, the addition of an exact form dp_L does not affect the circulation along closed curves, i.e. $\oint_C \eta = \oint_C \eta + dp_L$ for any closed curve C . Additionally, $\frac{\partial}{\partial t} \eta + \mathcal{L}_{\mathbf{u}} \eta = -dp_L$ implies that the circulation $\oint_{C_t} \eta_t$ is conserved if C_t is a closed curve advected by the fluid.⁶

2.2 Vorticity Equation

The *vorticity 2-form* is defined as $\omega = d\eta$ which measures local circulations. By taking the exterior derivative of (2a), applying $dd = 0$, and using the commutativity between $\mathcal{L}_{\mathbf{u}}$ and d , we obtain the *vorticity equation*

$$\frac{\partial}{\partial t} \omega + \mathcal{L}_{\mathbf{u}} \omega = 0. \quad (4)$$

Eq. (4) is often regarded as a formulation “equivalent to (2a).” It is the basis of the class of fluid solvers known as *vortex methods*. However, to fully establish the equivalence between (4) and (2a) (and to implement a vortex method), one must know how to reconstruct the velocity 1-form $\eta = \mathbf{u}^b \in \mathcal{V}^1$ from a given vorticity 2-form $\omega \in \text{im}(d) \cap \Omega^2(M)$ such that $d\eta = \omega$. The reconstruction problem is posed as follows.

Problem 1. *Given an exact $(k+1)$ -form $\omega \in \text{im}(d) \subset \Omega^{k+1}(M)$, find $\eta \in \mathcal{V}^k$ that solves $d\eta = \omega$.*

Unfortunately, the solution η may not be unique, depending on the fluid domain M . If $\zeta \in \ker(d) \cap \mathcal{V}^k$, readers can verify that $\eta + \zeta$ is also a solution to Problem 1. When $k = 1$, the subspace $\ker(d) \cap \mathcal{V}^1$ is the space of all closed and co-closed 1-forms (corresponding to curl-free and divergence-free vector fields) satisfying the co-Dirichlet

⁴The co-Dirichlet boundary condition is referred to as the *Neumann boundary condition* in [Schwarz 2006; Poelke and Polthier 2016]. For 1 form in 3D domains, [Abraham et al. 2012, §Hodge–de Rham theory] and [Zhao et al. 2019] refer to the Dirichlet and co-Dirichlet conditions as *normal* and *tangential* conditions respectively. We document how Dirichlet and co-Dirichlet boundary conditions relates to *normal* and *tangential* conditions for k -forms in 2D and 3D respectively in Tables 1 and 2.

⁵Here, the L^2 structure is $\langle\langle \alpha, \beta \rangle\rangle = \int_M \alpha \wedge \star \beta$.

⁶This is commonly known as the *Kelvin circulation theorem*. See more in [Nabizadeh et al. 2022].

boundary condition (corresponding to the no-through boundary condition for vector fields). In general, the space $\ker(d) \cap \mathcal{V}^k$ is the space of *co-Dirichlet harmonic forms*

$$\begin{aligned} \mathcal{H}_C^k(M) &= \ker(d) \cap \mathcal{V}^k \\ &= \left\{ h \in \Omega^k(M) \mid dh = 0, \delta h = 0, j^* \star h = 0 \right\}. \end{aligned} \quad (5)$$

Here, the subscript ‘‘C’’ indicates the co-Dirichlet boundary condition $j^* \star h = 0$.

2.2.1 Roadmap for Analyzing Problem 1. The standard method for reconstructing velocity from vorticity is through a streamfunction [Bridson 2015]. We show that this streamfunction and its boundary condition emerge naturally in the context of solving a particular solution to Problem 1. We first introduce the concept of *pseudoinverse* of the exterior derivative in Section 2.3. Then we apply the idea to the problem of velocity reconstruction from vorticity in Section 2.4.

2.3 Pseudoinverse of d

Definition 2. Define $d^+ : \Omega^{k+1}(M) \rightarrow \Omega^k(M)$ as the Penrose–Moore pseudoinverse of the exterior derivative $d : \Omega^k(M) \rightarrow \Omega^{k+1}(M)$ with respect to the L^2 -norms on $\Omega^k(M)$ and $\Omega^{k+1}(M)$. Explicitly, given $\beta \in \Omega^{k+1}$, let $P_{\text{im}(d)}\beta \in \text{im}(d) \subset \Omega^{k+1}$ be the orthogonal projection of β on $\text{im}(d)$:

$$P_{\text{im}(d)}\beta := d \left(\underset{\alpha \in \Omega^k(M)}{\text{argmin}} \|d\alpha - \beta\|^2 \right). \quad (6)$$

The pseudoinverse $d^+ \beta \in \Omega^k(M)$ is given by the least-norm solution

$$d^+ \beta := \underset{\alpha \in \Omega^k(M)}{\text{argmin}} \frac{1}{2} \|\alpha\|^2. \quad (7)$$

The general theory of pseudoinverses suggests that the pseudoinverse of a linear operator (d in our case) maps onto the orthogonal complement of the kernel of such a linear operator. Furthermore, the projection in (6) suggests that the pseudoinverse annihilates anything that is orthogonal to the image of the linear operator.

Proposition 2. The space of k -forms has an orthogonal decomposition

$$\Omega^k(M) = \ker(d) \oplus \text{im}(d^+), \quad (8a)$$

$$\Omega^{k+1}(M) = \text{im}(d) \oplus \ker(d^+). \quad (8b)$$

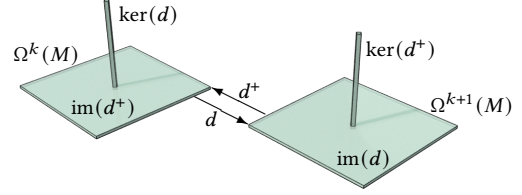
The orthogonal projectors to $\text{im}(d) \subset \Omega^{k+1}(M)$ and $\text{im}(d^+) \subset \Omega^k(M)$ are respectively

$$P_{\text{im}(d)} = dd^+, \quad P_{\text{im}(d^+)} = d^+d. \quad (9)$$

PROOF. See Appendix E.2. \square

Proposition 3. The subspaces $\text{im}(d^+) \subset \Omega^k(M)$ and $\text{im}(d) \subset \Omega^{k+1}(M)$ are isomorphic by the map $d|_{\text{im}(d^+)} : \text{im}(d^+) \rightarrow \text{im}(d)$ and its inverse $d^+|_{\text{im}(d)} : \text{im}(d) \rightarrow \text{im}(d^+)$.

PROOF. See Appendix E.3. \square



Next, we characterize $\text{im}(d^+)$.

Proposition 4. The image of d^+ is a subspace of \mathcal{V}^k . In particular:

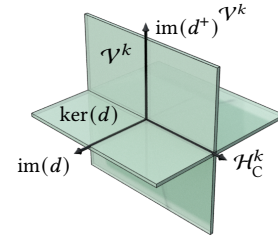
$$\text{im}(d^+) = \left\{ \delta\psi \mid \psi \in \Omega^{k+1}(M), j^* \star \psi = 0 \right\} = \delta(\ker(j^* \star)). \quad (10)$$

PROOF. See Appendix E.4. \square

Putting together Propositions 1, 2, 4 and Eq. (5), we obtain

Corollary 1. The space of k -forms are orthogonally decomposed into:

$$\Omega^k(M) = \overbrace{\ker(d)}^{\perp} \oplus \overbrace{\mathcal{H}_C^k(M)}^{\perp} \oplus \overbrace{\text{im}(d^+)}^{\perp}. \quad (11)$$



2.4 Stream-Form

In the context of fluids, for each vorticity 2-form $\omega \in \text{im}(d) \subset \Omega^2(M)$, a particular solution to Problem 1 is $\eta = d^+\omega$. By Proposition 4, this velocity 1-form is given by the codifferential $\delta\psi$ of some $\psi \in \Omega^2(M)$ that satisfies co-Dirichlet boundary condition. We call ψ the *stream-form*.

On a 2D domain, the stream-form $\psi \in \Omega^2(M)$ is typically represented as $\psi = \star\hat{\psi}$ by a scalar function $\hat{\psi} \in \Omega^0(M)$, called the *stream-function*. The co-Dirichlet boundary condition for ψ translates to the Dirichlet boundary condition $\hat{\psi}|_{\partial M} = 0$ for $\hat{\psi}$. For a streamfunction-represented velocity vector field, we have $\mathbf{u} = -\mathcal{J}\nabla\hat{\psi}$ where \mathcal{J} is the counterclockwise 90° rotation operator.

On a 3D domain, the stream-form $\psi \in \Omega^2(M)$ is usually represented by a vector field $\boldsymbol{\psi} \in \Gamma(TM)$ as $\psi = \star\boldsymbol{\psi}^\flat$. The vector field $\boldsymbol{\psi}$ is called vector potential, stream vector field, or just streamfunction. The velocity is given by $\mathbf{u} = \nabla \times \boldsymbol{\psi}$ and the boundary condition is that $\mathbf{n} \times \boldsymbol{\psi}|_{\partial M} = \mathbf{0}$, i.e. the stream vector field is normal to the boundary [Bridson et al. 2007].

2.4.1 Poisson Problem for Stream-Forms. To concretely construct $\psi \in \Omega^2(M)$ from $\omega \in \Omega^2(M)$ one solves a Poisson problem. For details related to this Poisson problem and its boundary conditions, see Appendix B.

2.4.2 Comments on 2D Streamfunctions. In many previous works involving 2D streamfunctions $\hat{\psi} \in \Omega^0(M)$, the streamfunctions are allowed to have constant but nonzero boundary conditions. The

velocity field $\eta = \delta(\star\hat{\psi})$ represented by this type of streamfunctions do carry the harmonic components. However, the existence of such streamfunctions only works for domains with special topology:

Proposition 5. *If a 2D domain M is the result of the removal of a few obstacles from a topological disk, then every $\eta \in \mathcal{V}^1$ is coexact.*

PROOF. See Appendix E.5. \square

In general, on a domain M that is a surface with a nonzero genus and with possibly a few obstacles removed, there are velocities that cannot be expressed by streamfunctions.

2.5 Summary

The vorticity data $\omega \in \text{im}(d) \subset \Omega^2(M)$ is in one-to-one correspondence with a stream-form-represented velocity field $d^+\omega \in \text{im}(d^+) \subset \mathcal{V}^1$ (Proposition 3). However, as shown in Corollary 1, the space $\text{im}(d^+)$ of stream-form-represented velocities is not the entirety of the space of all incompressible velocities \mathcal{V}^1 . The gap is the space of co-Dirichlet harmonic forms $\mathcal{H}_C^1(M)$ that is isomorphic to the 1st de Rham cohomology $H_{\text{dR}}^1(M) = \ker(d)/\text{im}(d)$, which is nontrivial whenever the domain is not simply-connected. In the context of Problem 1, $\mathcal{H}_C^1(M)$ is the space for non-uniqueness for the velocity reconstruction.

On a general non-simply-connected fluid domain, in order to pinpoint a velocity $\eta \in \mathcal{V}^1$ in terms of vorticity, one must use both the vorticity data ω and a co-Dirichlet harmonic form $h \in \mathcal{H}_C^1(M)$:

$$\eta = d^+\omega + h. \quad (12)$$

While the evolution equation of the vorticity ω is well-known, the evolution of the co-Dirichlet harmonic form h has been overlooked in all vorticity-streamfunction-based methods. We investigate the time-evolution of this harmonic component of Euler equations in Section 3.

2.6 Summary in Vector Calculus

Here we reiterate the above background in vector calculus via Tables 1 and 2 to gain perspective in the vector counterparts of propositions about differential forms.

The fluid velocity that we wish to study is the space of vector fields that are divergence free and satisfying no-through boundary condition $V := \{\mathbf{u} \mid \nabla \cdot \mathbf{u} = 0, (\mathbf{u} \cdot \mathbf{n})_{\partial M} = 0\}$. This is the vector calculus counterpart of \mathcal{V}^1 (Definition 1).

As documented in Tables 1 and 2, the vorticity $\omega = d\eta$ corresponds to the vorticity vector field $\mathbf{w} = \nabla \times \mathbf{u}$ in 3D or a vorticity scalar $w = \nabla \times \mathbf{u}$ in 2D. Section 2.3 introduces the notion of d^+ , which can be seen as taking the inverse of the curl operator. This “curl⁻¹” is more precisely the pseudoinverse curl^+ of the non-invertible curl operator. By Proposition 4, the image of the curl^+ operator is given by velocities represented by streamfunctions (Section 2.4) subject to a specific boundary condition

$$\text{im}(\text{curl}^+) = \{\nabla \times \boldsymbol{\psi} \mid (\mathbf{n} \times \boldsymbol{\psi})_{\partial M} = \mathbf{0}\} \quad \text{in 2D,} \quad (13a)$$

$$\text{im}(\text{curl}^+) = \left\{ -\mathcal{J}\nabla\hat{\psi} \mid \hat{\psi}|_{\partial M} = 0 \right\} \quad \text{in 3D.} \quad (13b)$$

Known as the boundary-aware Helmholtz–Hodge decomposition, Corollary 1 asserts that the space $\Gamma(TM)$ of vector fields can be

orthogonally decomposed into

$$\Gamma(TM) = \underbrace{\text{im}(\text{grad})}_{\ker(\text{curl})} \oplus \underbrace{H \oplus \text{im}(\text{curl}^+)}_V, \quad (14)$$

where H is the vector counterpart of (5) collecting harmonic vector fields satisfying the no-through boundary condition

$$H = \ker(\text{curl}) \cap V = \{\mathbf{h} \mid \nabla \cdot \mathbf{h} = 0, \nabla \times \mathbf{h} = 0, (\mathbf{h} \cdot \mathbf{n})_{\partial M} = 0\}. \quad (15)$$

Proposition 3 further shows that there is a one-to-one correspondence $\text{im}(\text{curl}^+) \cong \text{im}(\text{curl})$ between the space $\text{im}(\text{curl}^+)$ and $\text{im}(\text{curl})$. This means that the vorticity vector field \mathbf{w} in $\text{im}(\text{curl})$ (or scalar field w in 2D) is in one-to-one correspondence with a velocity field $\mathbf{u} = \text{curl}^+ \mathbf{w}$ in $\text{im}(\text{curl}^+)$ (or $\mathbf{u} = \text{curl}^+ w$ in 2D) represented by a streamfunction field $\boldsymbol{\psi}$ (or a scalar function $\hat{\psi}$ in 2D) as characterized in (13). In particular, as demonstrated in (14), the space V of all incompressible velocities is larger than the space $\text{im}(\text{curl}^+) \cong \text{im}(\text{curl})$ that can be captured by the vorticity data. The gap is the space H of harmonic vector fields with no-through boundary conditions. This gap H becomes nontrivial when the fluid domain is not simply-connected. Specifically, H is the kernel of the problem of reconstructing velocity from vorticity, which we discussed in Problem 1.

The decomposition (14) also reveals the difference between the velocity-based *pressure projection* and a vorticity-streamfunction solver in the context of advection-projection methods in fluid simulations. A pressure projection step removes $\text{im}(\text{grad})$ from $\Gamma(TM)$, keeping the information about the harmonic component H in V . This is consistent with the Euler equation. In contrast, a vorticity-streamfunction solver reconstructs the velocity using curl^+ from the vorticity data, effectively removing both $\text{im}(\text{grad})$ and H components from $\Gamma(TM)$. In particular, the vorticity-streamfunction solver leaves out the dynamics in the H component. As a result, different behaviors occur between these two methods on non-simply-connected domains as demonstrated in Fig. 1.

3 THEORY

The goal of this section is to develop the full equations of motion for both ω, h in (12). We first clarify the physical intuition to the harmonic component (Section 3.1). Next, we introduce the *Lamb form* (differential form counterpart of the *Lamb vector*), which is a central piece of the theory (Section 3.2). Finally, we derive the evolution equations for the harmonic part (Section 3.3), and explain the new physical law associated to it (Section 3.4).

3.1 Harmonic Part and Flux

In the fluid literature, the harmonic part of a velocity field is often loosely depicted as “flows around obstacles or holes.” Some parameterize the harmonic components by the *circulations* on a set of 1st homology basis (loops around obstacles) [Marsden and Weinstein 1983, §4; Elcott et al. 2007, §4.6]. While it is technically true that there is an isomorphism $H_1(M) \cong H_{\text{dR}}^1(M) \cong \mathcal{H}_C^1(M)$, different choices of loops lead to different parameterizations of the harmonic part of the velocity, even if the loops are only re-chosen within the

same homology class. This is because the mapping between the circulations and the strengths of harmonic components depends on an arbitrary choice of representative loops for $H_1(M)$ where we measure the circulations. For a consistent parameterization for the harmonic component, one must *fix* this arbitrary choice of loops. This is in contrast to picturing *flowing* loops as in the setup of Kelvin’s circulation theorem. In fact, Kelvin’s theorem on circulation conservation along *flowing* loops implies *nothing* about the conservation of the harmonic components [Thomson 1868].

As detailed below, we clarify a precise mapping between the harmonic component and a physical quantity of the fluid that is independent of the choice of artificial test geometry.

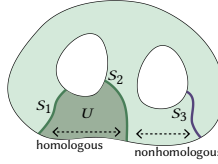
The harmonic component h of a velocity field η in (12) is directly related to the physical fluxes over cross-sectional surfaces.

3.1.1 Cross-sectional Fluxes. Fluid flux is measured over cross-sections of a fluid domain. A surface $S \in C_{n-1}(M)$ as an $(n-1)$ -chain is called *cross-sectional* if $\partial S \subset \partial M$ or $\partial S = \emptyset$. In relative homology theory, these cross-sectional surfaces are also known as *relatively closed surfaces*, or *relative cycles*, denoted by $S \subset Z_{n-1}(M, \partial M)$.

Definition 3. For each incompressible velocity field $\eta \in \mathcal{V}^1$ and cross-sectional surface $S \subset Z_{n-1}(M, \partial M)$, define

$$\text{FLUX}(\eta)(S) := \int_S \star \eta. \quad (16)$$

The definition of the FLUX operator can be written in vector calculus as well. In 3D, $\text{FLUX}(\mathbf{u})(S) := \iint_S \mathbf{u} \cdot \mathbf{n} \, dS$, where \mathbf{n} is the normal vector of surface S . In 2D, $\text{FLUX}(\mathbf{u})(S) := -\int_S (\mathcal{J}\mathbf{u}) \cdot dS$. The operator $\text{FLUX}: \mathcal{V}^1 \times Z_{n-1}(M, \partial M) \rightarrow \mathbb{R}$ is a bilinear form. Using the incompressibility conditions of $\eta \in \mathcal{V}^1$, one finds that $\text{FLUX}(\eta)(S_1) = \text{FLUX}(\eta)(S_2)$ whenever S_1, S_2 *coborder* a fluid region; that is $S_1 - S_2 \equiv \partial U \pmod{C_{n-1}(\partial M)}$ for some $U \in C_n(M)$, or that $S_1 - S_2 \in B_{n-1}(M, \partial M)$, or that S_1 and S_2 are *homologous*. Therefore, $\text{FLUX}(\eta)(\cdot)$ of any velocity data η assigns a well-defined flux data on each homology class $H_{n-1}(M, \partial M) = Z_{n-1}(M, \partial M)/B_{n-1}(M, \partial M)$ of cross-sections. The specific surface representing the cross-section from the homology is not important.



The following proposition summarizes the above discussion and formally treats FLUX as a map that sends velocity data to a set of flux data over the homology classes of cross-sections.

Proposition 6. For each $\eta \in \mathcal{V}^1$, the linear functional $\text{FLUX}(\eta): Z_{n-1}(M, \partial M) \rightarrow \mathbb{R}$ is well-defined over the relative $(n-1)$ -homology $H_{n-1}(M, \partial M) = Z_{n-1}(M, \partial M)/B_{n-1}(M, \partial M)$. As such we obtain a bilinear form $\text{FLUX}(\eta)([S]) := \text{FLUX}(\eta)(S)$ overloading on the same name:

$$\text{FLUX}: \mathcal{V}^1 \times H_{n-1}(M, \partial M) \rightarrow \mathbb{R}. \quad (17)$$

By currying, we may view the FLUX operator as a linear map that sends a velocity to the dual space of the relative $(n-1)$ -homology:

$$\text{FLUX}: \mathcal{V}^1 \xrightarrow{\text{linear}} H_{n-1}(M, \partial M)^*. \quad (18)$$

PROOF. See Appendix E.6. \square

Now, we show that (18) gives an isomorphism between the space $\mathcal{H}_C^1(M) \subset \mathcal{V}^1$ of harmonic components and the space $H_{n-1}(M, \partial M)^*$ of flux data on cross-sections. The first observation is that the flux data $\text{FLUX}(\eta)$ is independent of (and only of) the stream-form part $\text{im}(d^+)$ from vorticity. This property is particularly neat as $\text{im}(d^+)$ is the orthogonal complement of $\mathcal{H}_C^1(M)$ within \mathcal{V}^1 (cf. Corollary 1).

Proposition 7. $\ker(\text{FLUX}) = \text{im}(d^+)$.

PROOF. See Appendix E.7. \square

Moreover, every assignment of flux data is realizable by some co-Dirichlet harmonic form.

Proposition 8. $\text{FLUX}: \mathcal{V}^1 \rightarrow H_{n-1}(M, \partial M)^*$ is surjective.

PROOF. See Appendix E.8. \square

Diagrammatically, Propositions 7 and 8 can be summarized as a short exact sequence.

$$0 \rightarrow \text{im}(d) \xrightarrow{d^+} \mathcal{V}^1 \xrightarrow{\text{FLUX}} H_{n-1}(M, \partial M)^* \rightarrow 0. \quad (19)$$

The diagram shows that the space \mathcal{V}^1 of velocities is split into two “coordinates”: the stream-form part $\text{im}(d^+)$ and the harmonic part $\mathcal{H}_C^1(M)$. The stream-form part is parameterized by the vorticity data (Proposition 3), and the harmonic part is parameterized by the cross-sectional fluxes

$$\text{FLUX}|_{\mathcal{H}_C^1(M)}: \mathcal{H}_C^1(M) \xrightarrow{\cong} H_{n-1}(M, \partial M)^*. \quad (20)$$

In sum, each fluid state is described by two equally important pieces of information associated with concrete physical measurements. They are the vorticity field and the cross-sectional fluxes. With this endowment of physical meaning to fluid’s cohomology, we can discuss its expected behavior by drawing on physical intuition.

3.1.2 Unphysicality of Conservation of Harmonic Part. Many previous methods assume a time-constant harmonic part [Elcott et al. 2007, §4.5; Azencot et al. 2014, Eq. (1); Ando et al. 2015a, §3; Rioux-Lavoie et al. 2022, §4.1]. By Section 3.1.1, a time-constant harmonic part is equivalent to time-constant flux on every cross-section. Constant fluxes can lead to unphysical behavior. Imagine a traveling vortex pair (or vortex ring) initially distant from a cross-sectional surface, implying almost zero flux on the surface. Then the vortices will have a much more challenging time passing through that surface since the total flux over the surface is maintained at zero.

Fig. 7 shows a simple demonstration of this setup with the Kirchoff point vortex model computed using Biot–Savart integration. Kelvin’s method of reflection is employed for handling circular obstacles. To obtain unphysical dynamics with conserved harmonic components, one adds an additional point vortex at the center of each obstacle so that the flux between the obstacles stays zero. These additional compensating vortices repel the vortex pair in the physical domain.

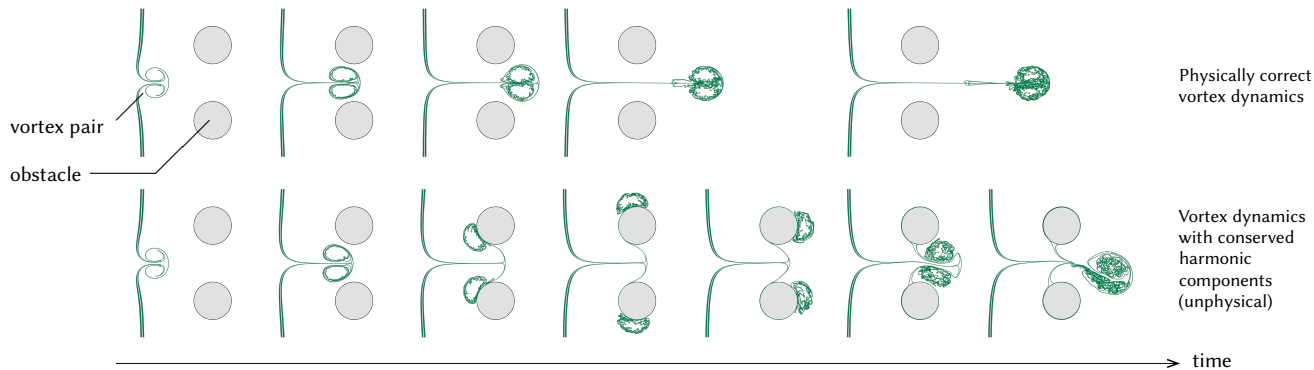


Fig. 7. A vortex pair approaching two circular obstacles in the plane. The physically correct behavior for the vortices is to pass through the space between the two obstacles (top row). An artificial fluid dynamics that preserves the harmonic component of the flow repels the vortices from passing between the obstacles (bottom row). The simulation is computed using Kirchoff’s point vortex dynamics with Kelvin’s method of reflection for handling circular obstacles.

In general, in a fluid solver where the harmonic components are constant, the approaching vortices induce a repulsing momentum that deflects the vortices. Section 5.2 includes a quantitative study (Fig. 15) of this phenomenon for a general fluid solver.

3.2 Lamb 1-Form

To describe the full evolution equation in Section 3.3, we first introduce a relevant quantity called the *Lamb form*.

Definition 4. For each velocity field $\eta = \mathbf{u}^\flat \in \mathcal{V}^1$, define the Lamb 1-form as

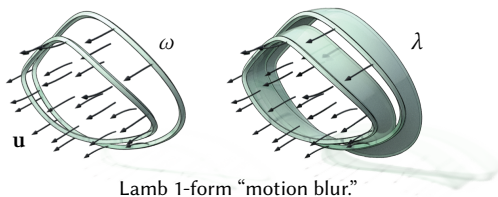
$$\lambda := -i_{\mathbf{u}}\omega, \quad \text{where } \omega = d\eta. \quad (21)$$

The vector counterpart of the Lamb form is the *Lamb vector* $\mathbf{l} := \lambda^\sharp$ given by

$$\mathbf{l} = \mathbf{u} \times \mathbf{w}, \quad \text{where } \mathbf{w} = \nabla \times \mathbf{u} \quad (22)$$

in 3D, and $\mathbf{l} = -w\mathcal{J}\mathbf{u}$ in 2D, where w is the scalar vorticity.

Geometrically, the Lamb 1-form, as a cloud of codimension-1 objects, is the resulting ribbon surfaces (or curve segments in 2D) from extruding vortex lines (or point vortices in 2D) along the (negative) velocity field for a unit of time. Since the vortices are just passively transported by the fluid flow as described by the Lie advection equation (4), one may think of λ as the trailing, or the “motion blur,” of the moving vortices.



We may rewrite Euler’s equation in terms of the Lamb form. Using Cartan’s formula $\mathcal{L}_{\mathbf{u}} = i_{\mathbf{u}}d + di_{\mathbf{u}}$, we rearrange (2a) into

$$\frac{\partial}{\partial t}\eta - \lambda = -dp_B, \quad (23)$$

where $p_B = p + \frac{1}{2}|\mathbf{u}|^2 = p_L + |\mathbf{u}|^2$ is called the *Bernoulli pressure* or the *stagnation pressure*. Similarly we can reexpress the vorticity

equation (4) (or by applying d to (23)) as

$$\frac{\partial}{\partial t}\omega = d\lambda. \quad (24)$$

The lamb form in (23) corresponds to the convection term in the Euler equations. Using 3D vector calculus, we have $\mathbf{l} = \mathbf{u} \times \mathbf{w} = \mathbf{u} \times (\nabla \times \mathbf{u})$. Recalling that the momentum equation of Euler equation is $\frac{\partial}{\partial t}\mathbf{u} + \mathbf{u} \cdot \nabla \mathbf{u} = -\nabla p$, we can plug in the vector identity $\mathbf{u} \cdot \nabla \mathbf{u} = \frac{1}{2}\nabla|\mathbf{u}|^2 - (\nabla \times \mathbf{u}) \times \mathbf{u}$ and $\mathbf{u} \times (\nabla \times \mathbf{u}) = \mathbf{l}$ to get $\frac{\partial}{\partial t}\mathbf{u} - \mathbf{l} = -\nabla(p + \frac{1}{2}|\mathbf{u}|^2)$ which is (23) in vector form.

Similarly, we can express (24) using 3D vector calculus and relate $d\lambda$ to the advection and the stretching term of the vorticity equation in vector form. Since λ is a 1-form, taking its exterior derivative corresponds to the curl of \mathbf{l} . Expanding the curl we have $\nabla \times \mathbf{l} = \nabla \times (\mathbf{u} \times \mathbf{w}) = \mathbf{u}(\nabla \cdot \mathbf{w}) - \mathbf{w}(\nabla \cdot \mathbf{u}) + (\mathbf{w} \cdot \nabla)\mathbf{u} - (\mathbf{u} \cdot \nabla)\mathbf{w}$. Note that \mathbf{u} and \mathbf{w} are divergence-free. Therefore, (24) can be written as $\frac{\partial}{\partial t}\mathbf{w} = (\mathbf{w} \cdot \nabla)\mathbf{u} - (\mathbf{u} \cdot \nabla)\mathbf{w}$. Rearranging terms, we obtain $\frac{D\mathbf{w}}{Dt} = (\mathbf{w} \cdot \nabla)\mathbf{u}$.

3.3 Equations of Motion

We are ready to lay down the governing equations for fluids’ harmonic components.

Let $m = \dim(\mathcal{H}_C^1(M)) = \dim(H_{\text{DR}}^1(M)) = \dim(H_1(M))$ be the dimension of the 1st homology of the domain.⁷ Let $(\zeta^1, \dots, \zeta^m)$, $\zeta^j \in \mathcal{H}_C^1(M)$, be a basis for the co-Dirichlet harmonic 1-forms. Note that the dual space of $\mathcal{H}_C^1(M)$ is the space of Dirichlet harmonic $(n-1)$ -forms

$$\mathcal{H}_D^{n-1}(M) := \{\xi \in \Omega^{n-1}(M) \mid d\xi = 0, \delta\xi = 0, j^*\xi = 0\} \quad (25)$$

via the following dual pairing

$$\mathcal{H}_C^1(M) \times \mathcal{H}_D^{n-1}(M) \rightarrow \mathbb{R}, \quad (\zeta, \xi) \mapsto \int_M \zeta \wedge \xi. \quad (26)$$

Determined uniquely by the basis $(\zeta^1, \dots, \zeta^m)$ for $\mathcal{H}_C^1(M)$ is a set of dual basis (ξ_1, \dots, ξ_m) for $\mathcal{H}_D^{n-1}(M)$ satisfying

$$\int_M \zeta^i \wedge \xi_j = \delta_j^i = \begin{cases} 1 & i = j \\ 0 & i \neq j, \end{cases} \quad \text{for all } i, j = 1, \dots, m. \quad (27)$$

⁷The number m is also known as the *1st Betti number*.

With the above sets of bases, we express a velocity field $\eta \in \mathcal{V}^1$ by a vorticity field $\omega \in \text{im}(d) \subset \Omega^2(M)$ and an m -tuple $\mathbf{c} = (c_1, \dots, c_m)^\top \in \mathbb{R}^m$ as

$$\eta = \eta_{(\omega, \mathbf{c})} = d^+ \omega + \sum_{j=1}^m c_j \zeta^j. \quad (28)$$

To extract the vorticity component, take the exterior derivative $\omega = d\eta$ as usual; to extract the coefficients \mathbf{c} , apply the dual pairing with the dual basis harmonic forms

$$c_i = \int_M \eta \wedge \xi_i, \quad i = 1, \dots, m. \quad (29)$$

Theorem 1. $\eta_{\omega, \mathbf{c}}$ evolves under the Euler equations (2) if and only if the vorticity ω and the coefficients \mathbf{c} evolve according to

$$\left\{ \begin{array}{l} \frac{\partial}{\partial t} \omega = d\lambda, \\ \frac{d}{dt} c_i = \int_M \lambda \wedge \xi_i, \quad i = 1, \dots, m, \end{array} \right. \quad (30a)$$

$$\left\{ \begin{array}{l} \frac{d}{dt} c_i = \int_M \lambda \wedge \xi_i, \quad i = 1, \dots, m, \end{array} \right. \quad (30b)$$

where λ is the Lamb 1-form for $\eta_{(\omega, \mathbf{c})}$.

One may take an orthonormal basis $(\zeta^1, \dots, \zeta^m)$ for $\mathcal{H}_C^1(M)$ by applying a Gram–Schmidt process or an economic QR decomposition on any other basis. In that case, $\xi_i = \star \zeta^i$. Let $\mathbf{h}_i = (\zeta^i)^\sharp$ be the vector counterparts of the harmonic forms. Then (30b) reads

$$\frac{d}{dt} c_i = \int_M (\mathbf{1} \cdot \mathbf{h}_i) dx = \begin{cases} \int_M -w \mathcal{J} \mathbf{u} \cdot \mathbf{h}_i dA & \text{in } 2D, \\ \int_M \det(\mathbf{u}, \mathbf{w}, \mathbf{h}_i) dV & \text{in } 3D. \end{cases} \quad (31)$$

PROOF. Eq. (30a) is the same as the vorticity equation (4) or (24). To obtain (30b), apply $\frac{d}{dt}$ to (29) to get $\frac{dc_i}{dt} = \int_M \frac{\partial \eta}{\partial t} \wedge \xi_i \stackrel{(23)}{=} \int_M (\lambda - dp_B) \wedge \xi_i = \int_M \lambda \wedge \xi_i$. The last equality is due to $\int_M dp_B \wedge \xi_i = \oint_{\partial M} (j^* p_B) \wedge (j^* \xi_i) - \int_M p_B d\xi_i = 0$ using the closedness and Dirichlet boundary condition of $\xi_i \in \mathcal{H}_D^{n-1}(M)$ (cf. (25)). \square

An earlier appearance of the time-evolution of the coefficients of any spectral basis under the Euler equations was in the velocity-based model reduction work by [Liu et al. 2015]. Our equation (31) is a special case of equation (7) from [Liu et al. 2015], since a basis for the harmonic component is a subset of a full spectral basis. We show that (30b) (or (31) in vector calculus) is the essential element for making vorticity-based solvers applicable to general domains, including non-simply connected ones. In the following subsection, by elucidating the theory behind cross-sectional flux, harmonic streamlines, and vortex lines, we demonstrate that (30b) leads to a conservation law with concrete physical and geometric meaning.

3.3.1 Practical Note.

Remark 1. In practice, to account for the missing dynamics of the fluid’s harmonic component, it is sufficient to “charge” the coefficients c_i ’s with the global aggregate sum of $(\mathbf{1} \cdot \mathbf{h}_i)$ across the domain, in conjunction with any vorticity-streamfunction solver.

Remark 2. Note that when the harmonic basis is orthonormal, the coefficients c_1, \dots, c_m do not directly represent the numeral values of the fluxes on domain’s cross-sections as described in Section 3.1. In the following Section 3.4.1, we describe which alternative basis to take in order to let the coefficients represent the fluxes directly.

Remark 3 (Physical units in an orthonormal setup). Including physical units, each ζ^i of an orthonormal harmonic basis for $\mathcal{H}_C^1(M)$ is of type $\zeta^i \in \Omega^1(M; \mathbb{R} m^{-n/2+1})$, and the dual basis is of type $\xi_i \in$

$\Omega^{n-1}(M; \mathbb{R} m^{n/2-1})$. That is, they are $\mathbb{R} m^{\mp n/2 \pm 1}$ -valued after being integrated over 1-chains and $(n-1)$ -chains respectively. The vector counterpart $\mathbf{h}_i = (\zeta^i)^\sharp$ has the unit of $m^{-n/2}$, and the coefficient c_i has the unit of $m^{n/2+1} s^{-1}$.

3.4 Flux Dynamics

In the remainder of the section, we expand on (30b) and elucidate its physical meaning by drawing a relation to cross-sectional fluxes. The purpose is to shed light to new physically and geometrically intuitive principles obeyed by incompressible fluids on multiply-connected domains. These principles may facilitate productions of qualitatively plausible fluid animations. Additional theoretic insights in terms of Hamiltonian mechanics are discussed in Section 6.

3.4.1 When the c_i ’s Become the Fluxes. As described in Section 3.1, the cross-sectional fluxes directly reflect the harmonic component of a velocity field. To make this relation more explicit, we pick a basis $(\zeta^1, \dots, \zeta^m)$ for \mathcal{H}_C^1 , different from an orthonormal one used in (31) and Section 3.3.1, so that the c_i ’s become the physical flux on cross-sections.

Let $S_1, \dots, S_m \in Z_{n-1}(M, \partial M)$ be a set of representative cross-sectional surfaces that forms a basis for $H_{n-1}(M, \partial M)$. Construct closed curves $C_1, \dots, C_m \in Z_1(M)$ such that their signed intersection products (denoted by $[\cdot \cap \cdot]$) are

$$[C_i \cap S_j] = \delta_{ij}. \quad (32)$$

Let $\delta_{C_i} \in \Omega^{n-1}(M)$ and $\delta_{S_j} \in \Omega^1(M)$ be the Dirac δ forms concentrated on these curves C_i ’s and surfaces S_j ’s. Define

$$\zeta^i := (1 - d^+ d) \star \delta_{C_i} \in \mathcal{H}_C^1(M), \quad (33a)$$

$$\xi_j := \star(1 - dd^+) \delta_{S_j} \in \mathcal{H}_D^{n-1}(M). \quad (33b)$$

The field ζ_i is the harmonic field “spread out from the concentrated current C_i ,” as the result of a stream-form part removal $(1 - d^+ d)$ from the current. The field ξ_j is the harmonic field “pumped out from the impulse at the cross-section S_j ,” as the result of the pressure projection $(1 - dd^+)$ (exact form removal) of the impulse.

Using vector calculus, $\zeta^i \in \mathcal{H}_C^1(M)$ and $\xi_j \in \mathcal{H}_D^{n-1}(M)$ can be represented as harmonic vector fields $\mathbf{Z}^i = \zeta^i$ and $\mathbf{X}_j = (\star^{-1} \xi_j)^\sharp$ respectively. They are constructed as

$$\mathbf{Z}^i := (1 - \text{curl}^+ \text{curl})(\star \delta_{C_i})^\sharp, \quad (34a)$$

$$\mathbf{X}_j := \text{PressureProjection}(\delta_{S_j}^\sharp). \quad (34b)$$

Note that $(n-1)$ -forms ξ_j ’s geometrically represent families of curves. These curves are the streamlines (integral curves) of the associated vector fields \mathbf{X}_j ’s. Therefore:

Definition 5 (Harmonic stream). We call ξ_j in (33b) the harmonic stream(line)s associated to a cross-sectional surface $S_j \in Z_{n-1}(M, \partial M)$.

Proposition 9. For ζ_i ’s and ξ_j ’s defined by (34), we have $\int_M \zeta^i \wedge \xi_j = \delta_j^i$. Moreover, for each velocity $\eta \in \mathcal{V}^1$ ($\mathbf{u} = \eta^\sharp \in V$), the coefficients c_j ’s in (28) are the fluxes through the cross-sectional surfaces:

$$c_j = \int_M \eta \wedge \xi_j = \int_M \mathbf{u} \cdot \mathbf{X}_j dV = \text{FLUX}(\eta)(S_j). \quad (35)$$

PROOF. See Appendix E.9. \square

Remark 4. The harmonic stream ξ_j constructed from a cross-sectional surface S_j by (33b) depends only on the equivalence class $[S_j] \in H_{n-1}(M, \partial M)$, i.e. it is independent of the particular choice of representative $S_j \in [S_j]$. In fact, $\xi_j = \text{FLUX}^\top([S_j])$ where FLUX^\top is the adjoint of the isomorphism $\text{FLUX}: \mathcal{H}_C^1(M) \rightarrow H_{n-1}(M, \partial M)^*$ in (19):

$$\begin{array}{ccc} \mathcal{H}_C^1(M) & \xrightarrow{\text{FLUX}} & H_{n-1}(M, \partial M)^* \\ \uparrow \text{dual space} & & \uparrow \text{dual space} \\ \xi_j \in \mathcal{H}_D^{n-1}(M) & \xleftarrow{\text{FLUX}^\top} & H_{n-1}(M, \partial M) \cong [S_j] \end{array} \quad (36)$$

Remark 5. Once the basis ξ_1, \dots, ξ_m is constructed from a generator basis S_1, \dots, S_m , one can construct the dual basis ζ^1, \dots, ζ^m through a simple QR-decomposition followed by a small matrix inversion without the hassle of building C_1, \dots, C_m . The detail of this process is described in Section 4.1.2

Remark 6 (Physical units for the flux setup). Similar to Remark 3, we discuss the physical units for the harmonic bases (34) and the coefficients. Each harmonic stream ξ_j is of type $\xi_j \in \Omega^{n-1}(M; \mathbb{R} m^{n-2})$, and its vector counterpart $(\star \xi_j)^\sharp$ has the unit of m^{-1} . The dual basis form ζ^i is of type $\zeta^i \in \Omega^1(M; \mathbb{R} m^{-n+2})$, whose vector counterpart $(\zeta^i)^\sharp$ has the unit of m^{-n+1} . The coefficients c_j has the unit of $m^n s^{-1}$, which is the unit of a total flux.

3.4.2 Fluxes and Linkings between Vortices and Harmonic Streamlines. Just as in the general theory (30b), the flux (35) through the j -th cross-sectional surface S_j has a rate of change given by

$$\frac{d}{dt} \text{FLUX}(\eta)(S_j) = \int_M \lambda \wedge \xi_j = \int_M \mathbf{1} \cdot \mathbf{X}_j dV. \quad (37)$$

In the codimensional geometric picture of differential forms, recall Section 3.2 that the Lamb 1-form λ is the collection of the “motion blur” ribbon surfaces trailing behind the flowing vortex lines, and ξ_j is the set of harmonic streamlines. The integrated wedge product $\int_M \lambda \wedge \xi_j$ is the total number of signed intersections between the motion blurs of vortex lines with the harmonic streamlines. In other words, $\int_M \lambda \wedge \xi_j$ is the rate at which vortex lines of ω cut through the harmonic streamlines of ξ_j . Therefore, $\int_M \lambda \wedge \xi_j$ is the rate of change of the “linking number” between the flowing vortex lines of ω and the static harmonic streamlines of ξ_j . We let this linking number be denoted by $\text{LINK}(\omega)(\xi_j)$ (whose subtle mathematical definition for general manifolds will be discussed later). As such, $\int_M \lambda \wedge \xi_j = \frac{d}{dt} \text{LINK}(\omega)(\xi_j)$.

Therefore, (37) is stating about a balancing relation between two rates of changes, one about the flux through S_j , and the other about $\text{LINK}(\omega)(\xi_j)$. We conclude this discovery in the following theorem.

Theorem 2. In an Euler fluid, for each cross-sectional surface S_j which generates harmonic streamlines ξ_j , the difference between fluid’s flux over S_j and the linking number between the vortex lines and harmonic streamlines

$$\text{FLUX}(\eta)(S_j) - \text{LINK}(\omega)(\xi_j) \quad (38)$$

is a constant of motion. (See Fig. 4.)

3.4.3 Linking in 2D Domains. In 2D, the vorticity 2-form ω is geometrically represented as a cloud of point vortices, instead of a cloud of vortex lines. In that case, $\text{LINK}(\omega)(\xi_j)$ is understood as the total winding number of the harmonic streamlines about the point vortices. Such linking/winding numbers can be defined for the following special 2D domains.

Suppose M has the topology of a disk with m obstacles removed. Then every cross-sectional curve S_j connects two of the $(m+1)$ -boundary components. Moreover, the associated $\xi_j \in \mathcal{H}_D^1(M)$ is exact (Proposition 5): There exists harmonic functions $U_j \in \Omega^0(M)$, unique up to a constant, such that

$$\xi_j = dU_j. \quad (39)$$

Geometrically, the harmonic streamlines of ξ_j are the level sets of the scalar potential U_j . Therefore, the winding number of these level lines around the vortex points of ω admits an explicit formula:

$$\text{LINK}(\omega)(\xi_j) = \int_M \omega U_j. \quad (40)$$

Corollary 2. For an Euler fluid on a disk with m obstacles, the difference between the fluid flux over S_j and the quantity (40) is a constant of motion.

Appendix D provides an analytical example for Corollary 2.

3.4.4 Linking in Euclidean Domains. When $M \subset \mathbb{R}^n$, every Dirichlet closed forms, such as ξ_j , is exact $\xi_j = d\alpha_j$ for some $\alpha_j \in \Omega^{n-2}(M)$ [Shonkwiler 2009; Zhao et al. 2019]. Fixing any representative potential α_j , the linking number admits an explicit formula:

$$\text{LINK}(\omega)(\xi_j) = \int_M \omega \wedge \alpha_j. \quad (41)$$

In 2D, α_j corresponds to a scalar function U_j in a 2D Euclidean domain, and the harmonic vector field \mathbf{X}_j , which is the vector counterpart of ξ_j , satisfies $\mathbf{X}_j = -\mathcal{J} \text{grad } U_j$. In a 3D Euclidean domain, α_j corresponds to a vector field \mathbf{a}_j with $\mathbf{X}_j = \text{curl } \mathbf{a}_j$. In terms of these vector calculus counterparts, we have

$$\text{LINK}(\omega)(\mathbf{X}_j) = \int_M \omega U_j dA \quad \text{in 2D,} \quad (42a)$$

$$\text{LINK}(\omega)(\mathbf{X}_j) = \int_M \omega \cdot \mathbf{a}_j dV \quad \text{in 3D.} \quad (42b)$$

3.4.5 Linking in General Domains. For general manifolds M , defining the linking number is trickier. To make sense of Theorem 2 we define the linking number between ω and ξ_j only through its variation with respect to ω . In that sense, Theorem 2 is understood as that this linking variation always balances out with the variation in the cross-sectional flux. For a detailed discussion on defining linking, see Appendix C.

4 IMPLEMENTATION

In the previous section, we derived the new dynamical equations for fluids’ harmonic parts (30b) and the underlying physical law (Theorem 2). In Section 5, we use numerical examples to demonstrate the effect of restoring such harmonic dynamics in vorticity-streamfunction solvers. The results will show that (30b) is crucial for reproducing realistic fluid dynamics in both 2D and 3D fluid

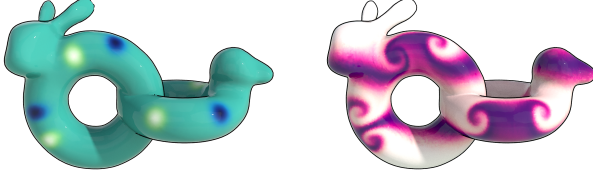


Fig. 8. Left: vortices on a surface with genus = 2 simulated using our method. Right: dye advected by the vortices.

simulations. In this section, we describe the implementation details for incorporating (30b) into existing state-of-the-art vorticity-streamfunction solvers. Our algorithm is not limited to the particular choice of solver we integrate with, but could be applied to different advection schemes.

For 2D examples, we adopt the method of *Functional Fluids* [Azencot et al. 2014] with a 4th-order Runge–Kutta time integration. This method is an accurate vorticity-streamfunction solver that applies to general triangulated surfaces with boundaries. The algorithm is implemented in SideFX’s Houdini 19.5, and the source code is available in the supplementary material.

For 3D examples, we employ *Covector Fluids* [Nabizadeh et al. 2022]. The original Covector Fluids solver is a velocity-based advection-projection method which provides base-line ground truth references. By replacing the pressure projection using a streamfunction solver [Ando et al. 2015a], the Covector Fluids solver becomes equivalent to a circulation-preserving vorticity-streamfunction method [Elcott et al. 2007] with a higher order advection bootstrapped by Back-and-Forth Error Correction and Compensation (BFEC) [Kim et al. 2005; Selle et al. 2008]. The algorithm is implemented in the C++ codebase provided by [Nabizadeh et al. 2022].

In each of these vorticity-streamfunction-based fluid simulators, we present algorithms for updating harmonic components.

4.1 2D Implementation on Triangle Meshes

We employ the *method of lines* for the 2D fluid simulations. That is, we spatially discretize the PDE (30), leaving a continuous-time ODE which is subsequently integrated using the 4th-order Runge–Kutta (RK4) method. The spatial discretization of the advective system on a triangle mesh follows [Azencot et al. 2014].

Let $M = (P, E, F)$ be a triangle mesh. A discrete vector field is a piecewise constant vector $\mathbf{u} = (\mathbf{u}_f \in T_f M)_{f \in F}$ assigned on the triangles. Each vector field \mathbf{u} is associated with a directional derivative operator $[\nabla_{\mathbf{u}}]: \mathbb{R}^{|P|} \xrightarrow{\text{linear}} \mathbb{R}^{|P|}$ that acts on a general function $f = (f_p)_{p \in P} \in \mathbb{R}^{|P|}$ by

$$([\nabla_{\mathbf{u}}]f)_p := \frac{1}{\sum_{f \triangleright p} A_f} \sum_{f \triangleright p} A_f \langle \mathbf{u}_f, (\text{grad } f)_f \rangle \quad (43)$$

where A_f is the area of triangle $f \in F$, and $(\text{grad } f)_f$ is the gradient of the piecewise linear interpolated function f in face $f \in F$.⁸ An explicit formula for the gradient is given by

$$(\text{grad } f)_f = \frac{1}{2A_f} \sum_{p < f} (-\mathcal{J}_f \mathbf{e}_{f,p}) f_p \quad (44)$$

⁸Another discrete function space that one may consider for taking gradients is the Crouzeix–Raviart finite element [Poelke and Polthier 2016]. We stick with the continuous piecewise linear element following [Azencot et al. 2014].

where \mathcal{J}_f is the 90° counterclockwise rotation within the tangent plane of the triangle f , and $\mathbf{e}_{f,p}$ is the (unnormalized) edge vector opposite to the point p across the triangle f .

In our system, each fluid state is given by a scalar vorticity field $w = (w_p \in \mathbb{R})_{p \in P}$ and a tuple of coefficients $\mathbf{c} = (c_i)_{i=1}^m \in \mathbb{R}^m$. With a pre-computed L^2 -orthonormal basis $(\mathbf{h}_1, \dots, \mathbf{h}_m)$ for $(\mathcal{H}_C^1(M))^\sharp$ (Section 4.1.1) we build a velocity field

$$\begin{aligned} \mathbf{u}_{(w,\mathbf{c})} &:= (d^+(\star w))^\sharp + \sum_{i=1}^m c_i \mathbf{h}_i \\ &= \text{VELOCITY}(w, \mathbf{c}; \mathbf{h}) \end{aligned} \quad (45)$$

using the algorithm below:

Algorithm 1 VELOCITY($w, \mathbf{c}; \mathbf{h}$): Velocity reconstruction in 2D

Input: Vorticity field $(w_p \in \mathbb{R})_{p \in P}$; harmonic coefficients $(c_i \in \mathbb{R})_{i=1}^m$; L^2 -orthonormal harmonic basis $(\mathbf{h}_{i,f} \in T_f M)_{i=1, f \in F}^m$.

- 1: $(\hat{\psi}_p)_{p \in P} \leftarrow \text{Solve } -\Delta \hat{\psi} = w, \hat{\psi}|_{\partial M} = 0;$ ▷ Appendix B.1
- 2: $(\mathbf{u}_f)_{f \in F} \leftarrow (-\mathcal{J}_f(\text{grad } \hat{\psi}))_f|_{f \in F};$
- 3: **for each** $i = 1, \dots, m$ **do**
- 4: $(\mathbf{u}_f)_{f \in F} \leftarrow (\mathbf{u}_f + c_i \mathbf{h}_{i,f})_f|_{f \in F};$

Output: $(\mathbf{u}_f)_{f \in F}$.

The reconstructed velocity (45) and the discrete directional derivative operator (43) allow us to express the right-hand sides of (30) discretely. In particular, (30) is discretized into an ODE:

$$\left\{ \begin{aligned} \frac{d}{dt}(w_p) &= -([\nabla_{\mathbf{u}_{(w,\mathbf{c})}}]w)_p, \quad p \in P, \\ \frac{d}{dt}(c_i) &= \sum_{f \in F} \langle \mathbf{l}_f, \mathbf{h}_{i,f} \rangle A_f, \quad i = 1, \dots, m. \end{aligned} \right. \quad (46a)$$

$$\quad (46b)$$

Here, the Lamb vector field $(\mathbf{l}_f \in T_f M)_{f \in F}$ is given by

$$\mathbf{l}_f = -\left(\frac{1}{3} \sum_{p < f} w_p\right) (\mathcal{J}_f \mathbf{u}_{(w,\mathbf{c}),f}). \quad (47)$$

Our main algorithm for 2D fluid simulator is Runge–Kutta integration for (46):

Algorithm 2 Fluid Solver on a Triangle Mesh

- 1: $\mathbf{h} = (\mathbf{h}_{i,f} \in T_f M)_{i=1, f \in F}^m \leftarrow$ An orthonormal basis for $\mathcal{H}_C^1(M)^\sharp;$ ▷ Section 4.1.1
 - 2: $w = (w_p \in \mathbb{R})_{p \in P} \leftarrow$ Initialize vorticity;
 - 3: $\mathbf{c} = (c_i \in \mathbb{R})_{i=1}^m \leftarrow$ Initialize harmonic coefficients;
 - 4: $\Delta t > 0 \leftarrow$ Set time step;
 - 5: **for each frame do**
 - 6: $\begin{bmatrix} w \\ \mathbf{c} \end{bmatrix} \leftarrow \text{RK4STEP}(\text{EVALRHS}, \begin{bmatrix} w \\ \mathbf{c} \end{bmatrix}, \Delta t);$
 - 7: **export** VELOCITY($w, \mathbf{c}; \mathbf{h}$);
 - 8: **function** EVALRHS($w = (w_p \in \mathbb{R})_{p \in P}, \mathbf{c} = (c_i \in \mathbb{R})_{i=1}^m$)
 - 9: $\mathbf{u} \leftarrow \text{VELOCITY}(w, \mathbf{c}; \mathbf{h});$ ▷ Alg. 1
 - 10: $\mathbf{l} \leftarrow$ Evaluate (47) using $w, \mathbf{u};$
 - 11: $\hat{w} = (\hat{w}_p)_{p \in P} \leftarrow$ Evaluate RHS of (46a) using w and $\mathbf{u};$
 - 12: $\hat{\mathbf{c}} = (\hat{c}_i)_{i=1}^m \leftarrow$ Evaluate RHS of (46b) using \mathbf{l} and $\mathbf{h};$
 - 13: **return** $(\hat{w}, \hat{\mathbf{c}});$
 - 14: **function** RK4STEP($F \in (\mathbb{T} \rightarrow \mathbb{T}), x \in \mathbb{T}, \Delta t \in \mathbb{R}$)
 - 15: $k_1 \leftarrow F(x); k_2 \leftarrow F(x + \Delta t/2 \cdot k_1);$
 - 16: $k_3 \leftarrow F(x + \Delta t/2 \cdot k_2); k_4 \leftarrow F(x + \Delta t \cdot k_3);$
 - 17: **return** $x + \Delta t/6 \cdot (k_1 + 2k_2 + 2k_3 + k_4);$
-

4.1.1 Orthonormal Basis for $\mathcal{H}_C^1(M)$. We generate a set of orthonormal basis for $\mathcal{H}_C^1(M)$ by constructing a basis based on (34) followed by a QR orthonormalization. On a triangle mesh, we first construct a basis (S_1, \dots, S_m) for $H_{n-1}(M, \partial M)$. Each S_i is a chain of dual edges (triangle strip) that is either closed or has both ends connected to ∂M . These relative homology generators S_j are found using a tree-cotree algorithm [Eppstein 2003; Erickson and Whittlesey 2005; Dlotko 2012].

Next, we build the discrete $\hat{\xi}_j \in \star^{-1}\xi_j \in \mathcal{H}_C^1(M)$ where $\xi_j \in \mathcal{H}_D^{n-1}(M)$ describes the harmonic stream described in Definition 5. For this process, we employ discrete exterior calculus (DEC) [Hirani 2003]. For each S_j , build a discrete primal 1-form that represents the impulse δ_{S_j} . That is, for a primal edge $e \in E$ crossed by S_j we set $(\delta_{S_j})_e$ to be ± 1 . The sign is chosen so that $\mathbf{d}_1 \delta_{S_j} = 0$, where \mathbf{d}_1 is the discrete exterior derivative operator (co-boundary operator) on 1-cochains. Each harmonic form $\hat{\xi}_j$ is built by the pressure projection $(1 - dd^+) \delta_{S_j}$ in the DEC sense.

Next, each $\hat{\xi}_j$ is interpolated into a piecewise constant vector field $(\hat{X}_j \in T_f M)_{f \in F}$ using Whitney interpolation [Bossavit 1998]. Now, we L^2 -orthonormalize $\hat{X}_1, \dots, \hat{X}_m$ with respect to the inner product structure $\langle \mathbf{u}, \mathbf{v} \rangle = \sum_{f \in F} \langle \mathbf{u}_f, \mathbf{v}_f \rangle A_f$. For each $j = 1, \dots, m$, pre-multiply the area factor $\tilde{X}_{j,f} = \sqrt{A_f} \hat{X}_{j,f}$, apply a QR factorization

$$\underbrace{\begin{bmatrix} | & & | \\ \mathbf{h}_1 & \cdots & \tilde{\mathbf{h}}_m \\ | & & | \end{bmatrix}}_{Q_{2|F| \times m}} \mathbf{R}_{m \times m} = \begin{bmatrix} | & & | \\ \tilde{\mathbf{X}}_1 & \cdots & \tilde{\mathbf{X}}_m \\ | & & | \end{bmatrix}. \quad (48)$$

Finally, we obtain an orthonormal basis $(\mathbf{h}_1, \dots, \mathbf{h}_m)$ for $\mathcal{H}_C^1(M)$ by $\mathbf{h}_{j,f} = \frac{1}{\sqrt{A_f}} \tilde{\mathbf{h}}_{j,f}$.

Alternatively, one can also use a randomized algorithm to obtain a set of orthonormal harmonic basis as explained in Section 4.2.1.

4.1.2 Harmonic Stream Basis for Flux Coefficients. While an orthonormal basis $(\mathbf{h}_1, \dots, \mathbf{h}_m)$ for $\mathcal{H}_C^1(M)$ is convenient in computation, its associated coefficients do not have direct physical meaning. Here, analogous to Section 3.4.1 we describe an alternative basis for $\mathcal{H}_C^1(M)$ so that c_1, \dots, c_m represent the total fluxes through S_1, \dots, S_m . Continuing (48), invert \mathbf{R} and reassemble the orthogonal basis $\tilde{\mathbf{h}}_1, \dots, \tilde{\mathbf{h}}_m$ into

$$\begin{bmatrix} | & & | \\ \tilde{\mathbf{Z}}_1 & \cdots & \tilde{\mathbf{Z}}_m \\ | & & | \end{bmatrix} = \begin{bmatrix} | & & | \\ \tilde{\mathbf{h}}_1 & \cdots & \tilde{\mathbf{h}}_m \\ | & & | \end{bmatrix} \mathbf{R}_{m \times m}^{-1}. \quad (49)$$

Define

$$(\mathbf{Z}_{i,f})_{f \in F} := \frac{1}{\sqrt{A_f}} \tilde{\mathbf{Z}}_i. \quad (50)$$

The bases (\mathbf{Z}_i) and (\hat{X}_j) are the discrete analogs of $(\zeta^i)^\sharp$ and $(\star^{-1}\xi_j)^\sharp$ defined in (34) respectively. Under these bases, one replaces \mathbf{h} by \mathbf{Z} in the velocity reconstruction (45) and Alg. 1; and one replaces \mathbf{h} by \hat{X} in the \mathbf{c} updates (46b). By doing so, the dynamics remains the same, but the coefficients c_1, \dots, c_m now represent the physical fluxes on the cross sections S_1, \dots, S_m .

4.2 3D Implementation on Staggered Grids

For 3D numerical examples, we integrate our algorithm to the codebase of Covector Fluids [Nabizadeh et al. 2022] for its equivalence to a circulation-preserving vorticity method. In particular, we replace the pressure projection step with a streamfunction solver applied to the vorticity. The discretization uses the standard MAC grid $M = (V, E, F, C)$ to store the variables. Similar to many other grid-based streamfunction solvers [Ando et al. 2015a; Chang et al. 2022], we store the velocity on grid faces, and store vorticity and streamfunction on grid edges. We explain solving the streamfunction Poisson problem in details in Appendix B. So far, this is a classical 3D vorticity-streamfunction solver that does not have the dynamics of the harmonic components.

In our method, we incorporate (31). We store our harmonic basis as m vector fields on the MAC grid faces, similar to the velocity fields. To evaluate the right-hand side $\int_M \det(\mathbf{u}, \mathbf{w}, \mathbf{h}_i) dV$ of (31), we interpolate the velocity $(u_f)_{f \in F}$, vorticity $(w_e)_{e \in E}$, and harmonic basis $(h_{i,f})_{f \in F}$ respectively into vector fields $(\mathbf{u}_c)_{c \in C}$, $(\mathbf{w}_c)_{c \in C}$, $(\mathbf{h}_{i,c})_{c \in C}$ that sit on the cell centers for easy local computations. With this discretization, we include the dynamics (31) by adding the following step in the main solver:

$$c_i \leftarrow c_i + \Delta t \sum_{c \in C} \det(\mathbf{u}_c, \mathbf{w}_c, \mathbf{h}_{i,c}) V_c, \quad (51)$$

where V_c is the cell volume. The harmonic coefficients are also used to reconstruct velocity after the streamfunction solver step. We summarize our overall procedure in Alg. 3.

Algorithm 3 3D Stream function solver with harmonic components

- 1: $\mathbf{h}_1, \dots, \mathbf{h}_m \leftarrow$ Generate an orthonormal basis for $\mathcal{H}_C^1(M, \partial M)^\sharp$;
 ▷ Section 4.2.1
 - 2: $c_1, \dots, c_m \leftarrow$ Initialize harmonic coefficients;
 - 3: $\mathbf{w} \leftarrow$ Initialize vorticity;
 - 4: $\Delta t \leftarrow$ Set time step;
 - 5: **for each** frame **do**
 - 6: $\boldsymbol{\psi} \leftarrow$ STREAMFUNCTIONPOISSONSOLVE(\mathbf{w});
 - 7: $\mathbf{v} \leftarrow$ CURL($\boldsymbol{\psi}$);
 - 8: $\mathbf{v} \leftarrow \mathbf{v} + \sum c_i \mathbf{h}_i$;
 - 9: $\mathbf{w} \leftarrow$ VORTICITYADVECTION(\mathbf{w} ; \mathbf{v} , Δt);
 - 10: $\boldsymbol{\lambda} \leftarrow$ CROSS(\mathbf{v} , curl \mathbf{v}) ▷ (24)
 - 11: **for each** $i = 1 \dots m$ **do**
 - 12: $\hat{c}_i \leftarrow$ INNERPRODUCT(\mathbf{h}_i , $\boldsymbol{\lambda}$) ▷ (31)
 - 13: $c_i \leftarrow c_i + \Delta t \hat{c}_i$; ▷ (51)
-

4.2.1 Generate Harmonic Basis in 3D. Methods for computing harmonic fields in a 3D domain are discussed in [Zhao et al. 2019]. In our case, we calculate an orthonormal basis for the harmonic components through a randomized algorithm. We generate m random vector fields where m is the dimension of $\mathcal{H}_C^1(M)$. We store these vector fields as flux on the faces of the staggered grid. We subtract the exact and co-exact components of these vector fields by applying $(1 - dd^+ - d^+d)$, i.e. by taking the difference between a standard pressure solve and a streamfunction solve. This procedure gives us m harmonic vector fields. These harmonic vector fields are

almost surely linearly independent. We then perform a QR decomposition (e.g. a Gram–Schmidt or a Householder process) to obtain an orthonormal basis for the harmonic components. See Alg. 4.

Algorithm 4 Generate an orthonormal basis for $\mathcal{H}_C^1(M, \partial M)$

- 1: $\mathbf{v}_1, \dots, \mathbf{v}_m \leftarrow$ Generate m random vector fields.
- 2: **for each** $i = 1, \dots, m$ **do**
- 3: $\tilde{\mathbf{h}}_i \leftarrow$ PRESSUREPROJECT(\mathbf{v}_i) – STREAMVELOCITY(curl \mathbf{v}_i).
- 4: $\tilde{\mathbf{h}}_i \leftarrow \sqrt{V} \tilde{\mathbf{h}}_i$; $\triangleright V = \text{voxel volume.}$
- 5: Construct $\mathbf{H} = \begin{bmatrix} \tilde{\mathbf{h}}_1 & \dots & \tilde{\mathbf{h}}_m \\ \vdots & & \vdots \end{bmatrix} \in \mathbb{R}^{3(\#\text{voxels}) \times m}$.
- 6: $\mathbf{Q} \in \mathbb{R}^{3(\#\text{voxels}) \times m}, \mathbf{R} \in \mathbb{R}^{m \times m} \leftarrow$ QR-DECOMPOSITION(\mathbf{H}).
- 7: **for each** $i = 1, \dots, m$ **do**
- 8: $\mathbf{h}_i \leftarrow \frac{1}{\sqrt{V}}$ (i -th column of \mathbf{Q}).

Output: $\mathbf{h}_1, \dots, \mathbf{h}_m$.

5 NUMERICAL EXAMPLES

In this section, we demonstrate the results from our incorporation of the dynamical harmonic components into vorticity-streamfunction fluid solvers for 2D surfaces (Alg. 2) and 3D scenes (Alg. 3).

5.1 2D Oscillating Fluxes with Closed Lamb Form

We design a setup so that the vortex dynamics (30a) vanish while a nontrivial evolution of the harmonic part (30b) is present. With this design, we single out the effect of the new equation (30b). We obtain the solution both numerically and analytically. In particular, the results demonstrate the necessity of (30b) for realistic fluid animation in contrast to previous methods.

5.1.1 Design Rationale. How do we keep the vorticity equation steady while keeping the harmonic part dynamic? A classically known result in fluid mechanics directly following from (23) is that the flow is steady ($\frac{\partial \eta}{\partial t} = 0$) if and only if the Lamb form is the gradient of the Bernoulli pressure $\lambda = dp_B$. Now, *what if we relax the condition of $\lambda \in \text{im}(d)$ to just $\lambda \in \text{ker}(d)$?* The closedness of λ will still ensure that the vorticity is steady ($\frac{\partial \omega}{\partial t} = 0$) using (30a). But such a non-exact closed λ , which contains harmonic components, can yield nontrivial dynamics in (30b), making the overall flow unsteady.

In 2D, a simple way to obtain a closed λ is to set vorticity constant, say $\omega = \star 1$. Then $\lambda = -i_0 \omega = -\star \eta$, which is closed since $\delta \eta = 0$. Next, we need to make sure λ is not exact. Observe that if the domain is the result of the removal of a few obstacles from a simply-connected disk, every $\lambda = -\star \eta$ is exact (Proposition 5). Therefore, the simplest non-trivial example is a surface with nonzero genus. The surface must also have at least one boundary component since a closed surface must have zero total vorticity.

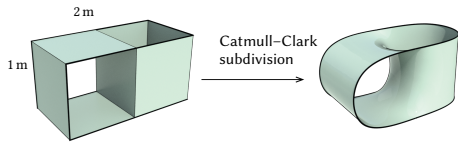


Fig. 9. A surface with genus = 1 and one boundary component.

5.1.2 Setup. Let the domain M be a surface with the topology of a torus with one disk removed. Fig. 9 illustrates the construction of the surface.

The domain has $m = \dim(\mathcal{H}_C^1(M)) = 2$. Set $\omega = w \star 1$, where $w \in \mathbb{R}(1/s)$ is a constant. Let (ζ^1, ζ^2) be an orthonormal basis for $\mathcal{H}_C^1(M)$. Its dual basis (ξ_1, ξ_2) for $\mathcal{H}_D^1(M)$ is given by $\xi_i = \star \zeta^i$.

The initial flow has nonzero harmonic components $(c_1, c_2)^\top|_{t=0} \neq (0, 0)^\top$. The velocity field generally takes the following form:

$$\eta^\# = w (d^+(\star 1))^\# + c_1 (\zeta^1)^\# + c_2 (\zeta^2)^\# \quad (52)$$

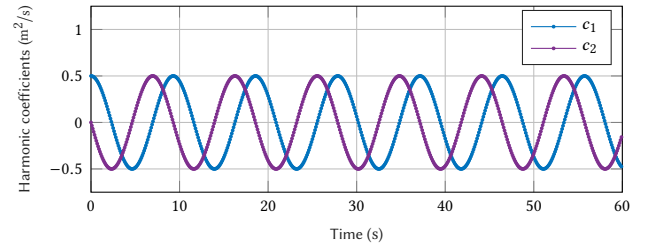


Fig. 10. Evolution of the coefficients of the harmonic components for the setup of Section 5.1.4, simulated by our method described in Section 4.1.

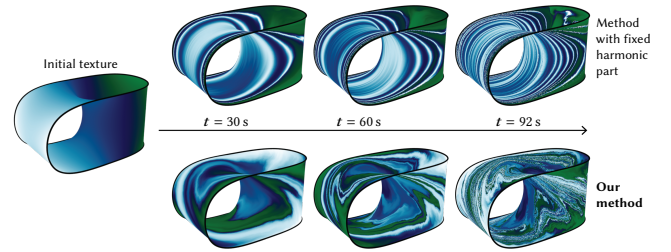


Fig. 11. Surface flows computed by the previous method [Azencot et al. 2014] and our method. The evolution of the harmonic component incorporated by our method is crucial for realistic flow animation (see video 02:26).

5.1.3 Analytic Solution. For constant vorticity $\omega = w \star 1$, the Lamb form is $\lambda = -w \star \eta = -w \star (d^+(\star 1) + c_1 \zeta^1 + c_2 \zeta^2) = w(d\hat{\psi} - c_1 \xi_1 - c_2 \xi_2)$, where $\hat{\psi} = \star \psi$ is the streamfunction. Since λ is closed, by (30a) the vorticity stays static. The only dynamics left is (30b), which now reads

$$\frac{dc_1}{dt} = w \int (d\hat{\psi} - c_1 \xi_1 - c_2 \xi_2) \wedge \xi_1 \stackrel{j^* \hat{\psi} = 0}{=} c_2 w \int_M \xi_1 \wedge \xi_2 \quad (53)$$

and similarly

$$\frac{dc_2}{dt} = -c_1 w \int_M \xi_1 \wedge \xi_2. \quad (54)$$

That is, $(c_1, c_2)^\top$ evolves in a simple harmonic oscillation

$$\frac{d}{dt} \begin{bmatrix} c_1 \\ c_2 \end{bmatrix} = \mu w \begin{bmatrix} 0 & 1 \\ -1 & 0 \end{bmatrix} \begin{bmatrix} c_1 \\ c_2 \end{bmatrix}, \quad \mu := \int_M \xi_1 \wedge \xi_2 = \int_M \zeta^1 \wedge \zeta^2, \quad (55)$$

which has an explicit solution

$$\begin{bmatrix} c_1(t) \\ c_2(t) \end{bmatrix} = \begin{bmatrix} \cos(\mu w t) & \sin(\mu w t) \\ -\sin(\mu w t) & \cos(\mu w t) \end{bmatrix} \begin{bmatrix} c_1(0) \\ c_2(0) \end{bmatrix}. \quad (56)$$

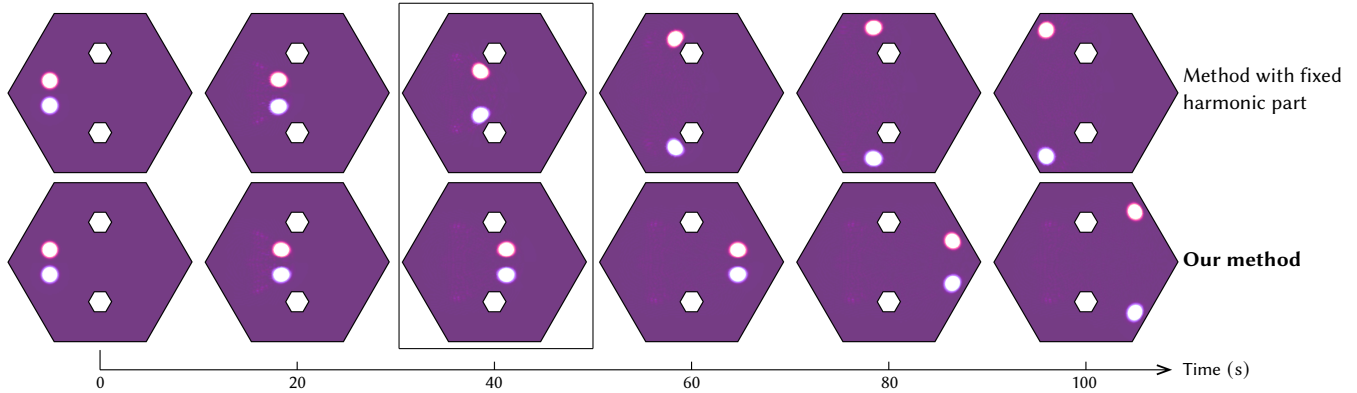


Fig. 12. The time-evolution (from left to right) of a vortex pair moving through a fluid domain with two small hexagonal obstacles, simulated by [Azencot et al. 2014] (top) and our method (bottom) (see video 01:00).

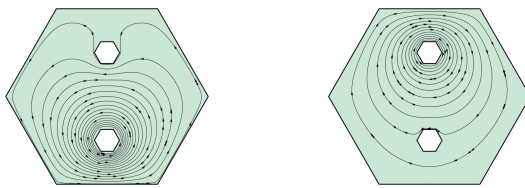


Fig. 13. A harmonic basis for a hexagonal disk with 2 hexagonal holes removed.

The frequency μw of the oscillation is proportional to the background vorticity $w \in \mathbb{R}(1/s)$ and a dimensionless number μ depending on the geometry. Note that the construction of μ relies only on the \star on 1-forms. Hence μ depends only on the *conformal type* of the surface [Soliman et al. 2021].

5.1.4 Numerical Results. We apply our fluid solver (Alg. 2) to the configuration of Section 5.1.2. We set $w = 2 s^{-1}$, $c_1(0) = 0.5 m^2/s$ and $c_2(0) = 0 m^2/s$. The solver is set with time discretization $\Delta t = 0.1 s$. The result is compared against the previous vorticity-streamfunction method on surfaces [Azencot et al. 2014], which is our algorithm without (30b).

Fig. 10 shows the numerical values of c_1 and c_2 over time. In particular, they agree with the analytical solution $c_1(t) = 0.5 \cos(\mu w t)$, $c_2(t) = -0.5 \sin(\mu w t)$ (cf. (56)). Previous methods that keep $(c_1, c_2) = (0.5, 0)$ constant over time would lead to a vastly different flow both quantitatively and qualitatively. In Fig. 11, we advect colors to compare the resulting flow map of the previous method [Azencot et al. 2014] and ours. In [Azencot et al. 2014] the inertia is not correctly transferred, creating an unnatural laminar texture that is not turned by the background vorticity. The problem is solved in our method which incorporates the evolution of the harmonic components.

5.2 2D Vortex Pair Between Obstacles

Let the domain M be a flat hexagonal disk with two hexagonal holes removed, similar to an ocean basin with two islands. The dimension of its 1st relative homology is two, and therefore the dimension of the harmonic basis is two, as illustrated in Fig. 13.

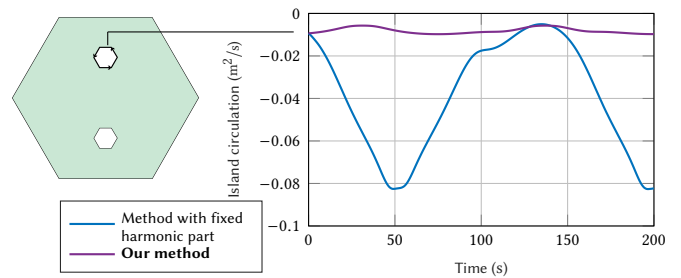


Fig. 14. Circulation around a boundary component in Fig. 12.

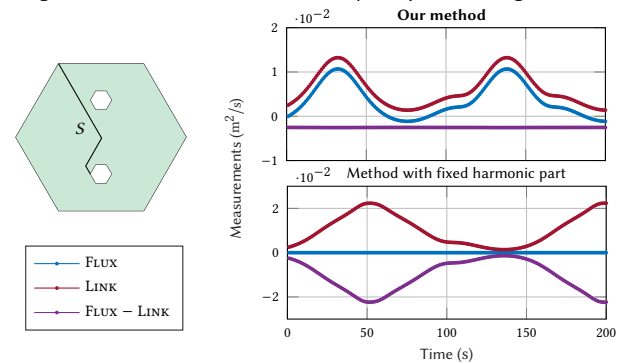


Fig. 15. FLUX, LINK, and FLUX - LINK for a cross-section S in Fig. 12.

We set a pair of vortices with opposite values as shown in Fig. 12 at $t = 0 s$. In principle, we expect the traveling vortex pair to pass through the space between the islands. However, using the method [Azencot et al. 2014] with a fixed harmonic part, the two vortices do not pass through. Instead, they turn around and go back in the opposite direction when they approach the islands. This unphysical behavior is due to a vanishing total flux along the curve connecting the two holes maintained by the fixed harmonic part. Using our method which includes (30b), the vortices pass through as expected. Fig. 12 shows the dynamics of the vortices over time for both methods.

In addition to inspecting the vortex motion, we also determine the correctness of the competing methods quantitatively. In Fig. 14

we measure the circulations around one of the islands over time for both methods. Since the flow is always tangential to the boundary, the boundary curve of the island that flows with the fluid will stay as the same boundary curve. In particular, Kelvin’s circulation theorem or *island rule* [Godfrey 1989; Pedlosky et al. 1997] applies. The circulation along the island boundary should be conserved. As shown in Fig. 14, our method better conserves the circulation, while the method with a fixed harmonic part violates this conservation law. In Fig. 15, we consider a cross-section S , and measure the corresponding FLUX, LINK, and FLUX – LINK. Using our method, FLUX – LINK is a conserved quantity. In contrast, using the method with a fixed harmonic part, the flux is always zero, and FLUX – LINK is not conserved.

5.3 3D Examples on Non-simply-connected Domains

Similar to the 2D examples, when one does not incorporate the dynamics of harmonic components into vorticity-streamfunction methods, unphysical behaviors occur in a domain with non-trivial topology. We set up three experiments by introducing different obstacles (fan, torus, and pillars) into a closed box domain, making the domain non-simply connected (see Fig. 16).

In Experiment 1 (Fan) we place a torus-shaped fan in the domain which raises the dimension of its 1st cohomology to one. Experiment 2 (Torus Rock) is staged with a torus-shaped rock submerged in an aquarium. Similar to the previous setup, the 1st cohomology’s dimension is one. Experiment 3 (Pillars Rock) is also set in an aquarium, but the obstacles are two pillars. Since the pillars touch both the top and the bottom of the boxed domain, the dimension of the 1st cohomology is two. We illustrate the harmonic basis for Experiment 1 (Fan) and Experiment 3 (Pillars Rock) in Fig. 17.

We run our experiments on uniform staggered grids with a voxel resolution of $150 \times 75 \times 75$ in a box size of $10 \times 5 \times 5 \text{ m}^3$. The timestep duration is set to $1/24$ seconds with two substeps per frame. A vortex ring of radius 0.4 m is initialized to face in the positive x -direction with strength $1.6 \text{ m}^2/\text{s}$. As mentioned in Section 4, for 3D flows, we use Covector Fluids solver [Nabizadeh et al. 2022] as our velocity-based method reference (right). We replace the pressure projection step with a streamfunction Poisson solver as the results which represent classical methods with fixed harmonic parts (left). Our method includes the evolution of harmonic parts (30b) (middle).

Fig. 1, and Fig. 16 demonstrate the results of the three experiments detailed above. A significant amount of vorticity is trapped by the obstacles when one uses a traditional method that fixes harmonic parts (left). This behavior does not match the results in the velocity-based method reference (right). In particular, in the result of Experiment 1 (Fan) computed by the method fixing harmonic parts (left), only a small portion of the vortex passes through the fan while the majority of the vortex moves in the opposite direction to compensate for a vanishing total flux across the fan. Using our method (middle), the vortex passes through the obstacles with an overall dynamical behavior similar to the velocity-based method reference (see video).

In conclusion, the numerical examples demonstrate that a classical vorticity-streamfunction solver can generate incorrect flow patterns. Our method for including the dynamics of harmonic parts solves this problem.

6 HAMILTONIAN FORMULATION

One of the highlights in the theory of Hamiltonian Fluid Mechanics is interpreting the vorticity equation (4) or (30a) as a *reduced* infinite-dimensional Hamiltonian system in classical mechanics. In this final discussion section, we extend the Hamiltonian description to include our new equation (30b) of the time-evolution of the harmonic coefficients. Readers can find introductions to the most common Hamiltonian formulation for fluid dynamics in [Salmon 1988] using elementary continuum mechanics, [Morrison 1998] using non-canonical transformations, or [Arnold 1966; Marsden and Weinstein 1983; Arnold and Khesin 1998] using group theory.

Background. The setup for a Hamiltonian formulation involves several steps. One first establishes a set of variables that describe the state of the physical system. The space of all possible states is called the *phase space* \mathcal{M} . One then describes a symplectic structure. A *symplectic structure* is a non-degenerate closed 2-form $\sigma \in \Omega^2(\mathcal{M})$ that encodes the interrelation among the variables such as position-momentum pairing. When the phase space has a symplectic structure, it is called a *symplectic manifold*. In many weaker cases including the case of fluids, the phase space \mathcal{M} is merely foliated into many symplectic submanifolds called *symplectic leaves*. Such a phase space is called a *non-canonical space* or a *Poisson manifold* [Weinstein 1998]. Finally, one describes the final dynamical system by defining a Hamiltonian function $H: \mathcal{M} \rightarrow \mathbb{R}$, which expresses the total energy of the system for each state. The equation of motion (called the *Hamiltonian flow*) is derived as the *symplectic gradient flow*⁹ of the Hamiltonian function H . In the case where \mathcal{M} is only a Poisson manifold instead of a single symplectic manifold, the Hamiltonian flow just flows within each symplectic leaf. Any function $C: \mathcal{M} \rightarrow \mathbb{R}$ defined on the phase space (such as a physical measurement) is called a *Casimir* if C is constant on each symplectic leaf; *i.e.* symplectic leaves are contained in the level sets of C . As a direct consequence, every Hamiltonian flow (of any Hamiltonian function) is a dynamical system where the measurement C is a constant of motion.

The above setup is typically easy to describe for particle systems and their continuum limits, as one may define the positions and momenta as the obvious ones for each particle. The non-trivial aspect about Hamiltonian Fluid Mechanics is after the so-called *reduction* by sorting out the *particle-relabeling symmetry* [Salmon 1988]. After the reduction, the position and momentum of each individual particle are no-longer parts of the coordinates of the phase space. Instead, what naturally emerges is that the phase space for incompressible fluids is the quotient space $\mathcal{M} = \Omega^1(M)/d\Omega^0(M)$ of velocity 1-forms modulo an exact form (d of Lagrangian pressure) [Arnold and Khesin 1998, Theorem I.7.5]. In fact, this phase space is a Poisson manifold with symplectic leaves given by the orbits of Lie transportations of velocity 1-forms under any volume-preserving flow maps (*i.e.* the pullback of velocity 1-forms under the inverse of the flow maps). In particular, Kelvin’s circulation theorem can be thought of as a Casimir-typed conservation law. A more concrete example of Casimir in a 3D incompressible fluid is the *helicity* $\int_{\mathcal{M}} \eta \wedge \omega$ that measures the self-linking number of vortex lines.

⁹Symplectic gradient flow is defined identically to gradient descent flow with inner product structure $\langle \cdot, \cdot \rangle$ replaced by the symplectic form $\sigma(\cdot, \cdot)$.

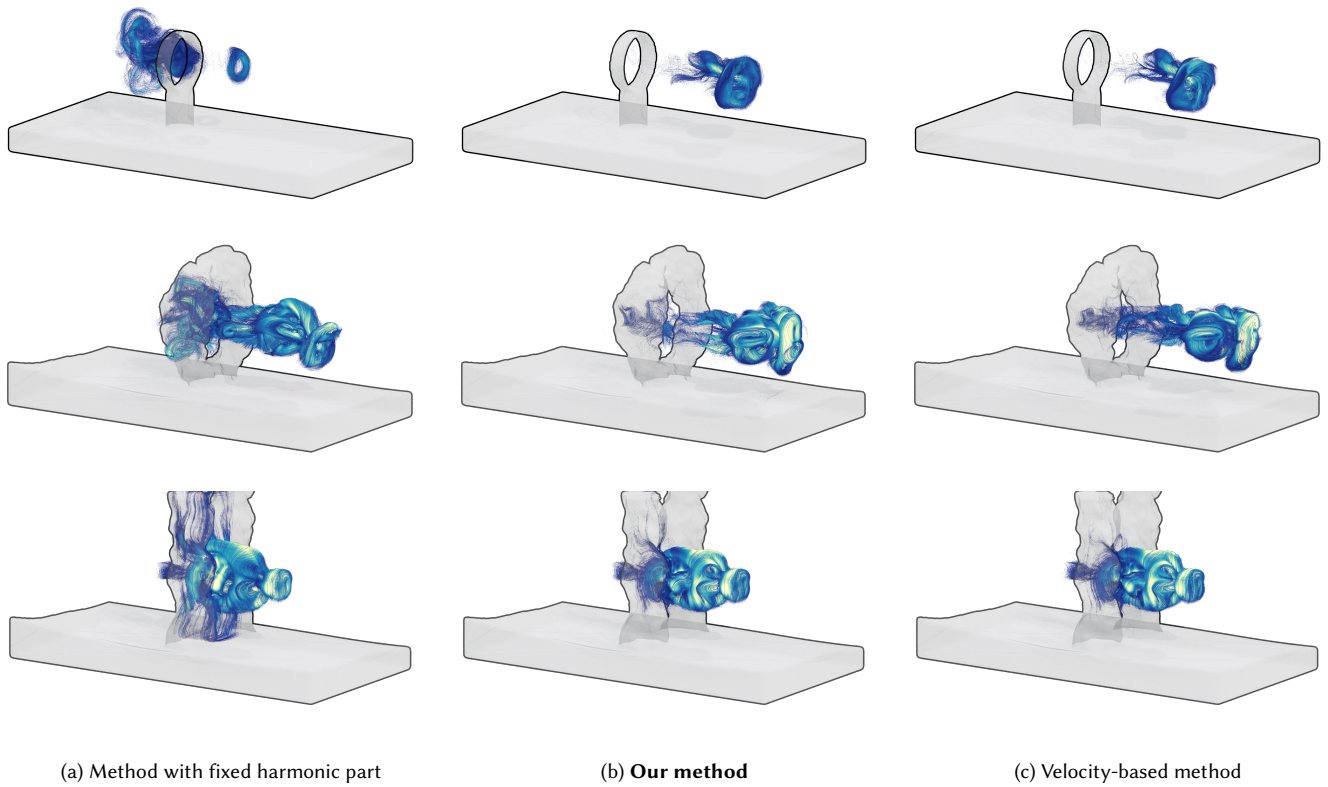


Fig. 16. Visualizations of vorticities from Experiment 1 (Fan), Experiment 2 (Torus Rock), and Experiment 3 (Pillars Rock). Note that using the method with a fixed harmonic part, the vorticity appears to be trapped by the obstacles, especially in Experiment 1 (Fan). Our method resolves this issue and produces visually similar results to ground truth (velocity-based advection-projection scheme).

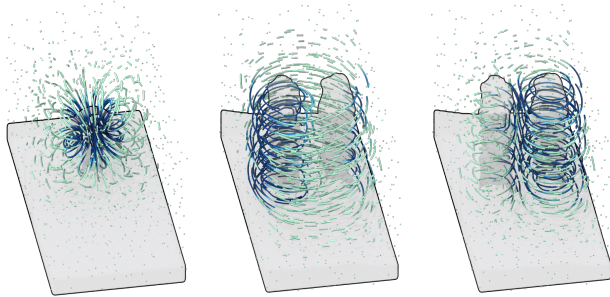


Fig. 17. Harmonic bases for Experiment 1 (Fan) in the left figure, and Experiment 3 (Pillars Rock) in the middle and right figures. Note that our domain is inside a closed box, but we only include the bottom side of the box to better visualize the harmonic fields inside.

To make the quotient space $\mathcal{M} = \Omega^1(M)/d\Omega^0(M)$ less abstract, a common practice is to describe $\mathcal{M} = \text{im}(d_1) \subset \Omega^2(M)$ as the space of vorticity fields (by assuming there is no cohomology component) [Marsden and Weinstein 1983, §4]. Such a treatment is attractive, since vorticity has a concrete physical meaning, and the Hamiltonian flow ($H = \text{total kinetic energy}$) on the vorticity variable directly

yields the familiar vorticity equation (4) or (30a). The drawback is of course it does not describe fluids on non-simply-connected domains.

Our Modification. Similar to our Theorem 1, the fluid state is described by both vorticity $\omega \in \text{im}(d_1) \subset \Omega^2(M)$ and coefficients of harmonic components $\mathbf{c} = (c_i)_{i=1}^m \in \mathbb{R}^m$. Importantly, as described in (19) and Section 3.4.1, the coefficients \mathbf{c} have the concrete physical meaning of flux through cross-sections S_1, \dots, S_m of the domain. Recall that each cross section S_i is associated with a harmonic field ξ_i defined in (33b). Our phase space \mathcal{M} is given by the coordinate of vorticity data and the flux data:

$$\mathcal{M} := \text{im}(d_1) \times \mathbb{R}^m = \{(\omega, \mathbf{c}) \mid \omega \in \text{im}(d_1), \mathbf{c} \in \mathbb{R}^m\}. \quad (57)$$

This phase space is a Poisson manifold. We describe the Poisson structure by defining its symplectic foliation as follows. A tangent vector $(\dot{\omega}, \dot{\mathbf{c}})|_{(\omega, \mathbf{c})} \in T_{(\omega, \mathbf{c})}\mathcal{M}$ at state $(\omega, \mathbf{c}) \in \mathcal{M}$ is *tangent to the symplectic leaf* if it takes the following form

$$\dot{\omega} = -d_i X \omega, \quad \dot{c}_i = \int_M (-i_X \omega) \wedge \xi_i \quad (58)$$

for some divergence-free vector field $X \in \Gamma(TM)$. One can check that the distribution of tangent subspaces (58) is integrable¹⁰ and hence form a foliation. We define the symplectic form σ on the symplectic

¹⁰A simple way to verify the integrability of the distribution (58) is to realize that the reconstructed velocity $\eta_{(\omega, \mathbf{c})} := d^* \omega + \sum_i c_i \zeta^i$ has the corresponding motion

leaf: For every two tangent vectors $(\dot{\omega}, \dot{c}) = (-di_X\omega, \int_M(-i_X\omega) \wedge \xi)$, $(\dot{\omega}, \dot{c}) = (-di_Y\omega, \int_M(-i_Y\omega) \wedge \xi)$ tangent to the leaf (where $X, Y \in \Gamma(TM)$ are arbitrary divergence-free vector fields),

$$\sigma_{(\omega, c)}((\dot{\omega}, \dot{c}), (\dot{\omega}, \dot{c})) := \int_M \omega(X, Y) \star 1. \quad (59)$$

This symplectic form is the same as the one defined in the literature [Marsden and Weinstein 1983] but now lifted to a larger space (57). Note that the definition (58) ensures that $\text{FLUX}(\eta)(S_i) - \text{LINK}(\omega)(\xi_i)$ is always invariant under any variation along a symplectic leaf. We elaborate on the variation of LINK in Appendix C. In particular, $\text{FLUX}(\eta)(S_i) - \text{LINK}(\omega)(\xi_i)$ is a Casimir for each $i = 1, \dots, m$ (cf. Theorem 2). Finally, one may verify that our full equation (30) is the Hamiltonian flow of the total kinetic energy

$$H(\omega, c) := \int_M \frac{1}{2} |d^+\omega + \sum_{i=1}^m c_i \xi_i|^2 \star 1. \quad (60)$$

In summary, the above equations complete the vorticity-based Hamiltonian description of incompressible fluid dynamics in domains with general topology. This mathematical framework may serve as a foundation for future research in mathematical fluid mechanics.

7 CONCLUSION

In this paper, we tackle a long-existing problem in the vorticity-streamfunction formulation of incompressible Euler fluids on non-simply-connected domains. We demonstrate that the dynamics for the harmonic (cohomology) components of incompressible Euler fluids can be described by (30b) (Theorem 1). This has been overlooked by previous vorticity-streamfunction solvers. We give a simple and practical algorithm in Section 4 that easily incorporates such dynamics into previous vorticity-streamfunction solvers.

Our numerical examples (Section 5) demonstrate that it is necessary to include the additional equations in a vortex solver to avoid unphysical artifacts in fluid animations.

The proposed algorithm for 2D surface simulation (Alg. 2) is particularly significant because while vorticity-based methods (involving only scalar advectons) are much more straightforward to compute on a 2D surface domain compared to a velocity-based solver (involving covariant vector advection), previous vorticity-based surface fluid solvers do not include the dynamics of the harmonic components. Our Alg. 2 is the first vortex solver that is consistent with the Euler equations on surfaces with arbitrary topology.

We also find a new physical conservation law associated with the new evolution of harmonic components (Theorem 2). We describe our new equation as a Hamiltonian system on the state space coordinated by the vorticity and the cross-sectional fluxes (Section 6). Compared to previous editions of Hamiltonian formulation for incompressible Euler flows, the new framework does not omit the cohomology and each variable is a physically meaningful measurement. The mathematical investigations have also led us to discover new Casimir invariants as well as interesting analytic flows, e.g. the example presented in Section 5.1. It would be exciting to explore if this new conserved quantity that we discovered could serve as the foundation for new algorithms in the future.

This paper leaves a few open questions that are beyond our current investigation. We only work on inviscid Euler fluids on a fixed

of $\dot{\eta} = -\mathcal{L}_X \eta$ modulo $\text{im}(d_0)$. Hence, (58) is just the tangent vectors to the known symplectic leaves in $\Omega^1(M)/d\Omega^0(M)$. In particular, the distribution (58) is integrable.

oriented Riemannian manifold. In particular, we do not consider moving obstacles or that the domain is an evolving surface. Expanding our analysis to moving domains can yield new perspectives to the studies of underwater swimmers and solid-vortex interactions [Vankerschaver et al. 2009; Weißmann 2014]. Lastly, *what is the effect of viscosity? What if the domain has changing topology? What if the domain is non-orientable?* We expect exciting research answering these and related questions in the near future.

ACKNOWLEDGMENTS

This work was funded by NSF CAREER Award 2239062 and UC San Diego Center for Visual Computing. Additional support was provided by the WiGRAPH Rising Stars Program, SideFX Software, and Activision Blizzard. The authors would like to thank Prof. Ulrich Pinkall, Prof. Peter Schröder, and Mark Gillespie for insightful discussions and Benjamin Lindsay for editorial assistance.

REFERENCES

- Ralph Abraham, Jerrold E Marsden, and Tudor Ratiu. 2012. *Manifolds, tensor analysis, and applications*. Vol. 75. Springer Science & Business Media.
- Christopher R Anderson. 1989. Vorticity boundary conditions and boundary vorticity generation for two-dimensional viscous incompressible flows. *J. Comput. Phys.* 80, 1 (1989), 72–97.
- Ryoichi Ando, Nils Thuerey, and Chris Wojtan. 2015a. A Stream Function Solver for Liquid Simulations. *ACM Transactions on Graphics (TOG)* 34, 4 (2015), 53:1–52:9.
- Ryoichi Ando, Nils Thuerey, and Chris Wojtan. 2015b. A Hindsight on the Stream Function Solver for Liquid Simulation (Errata for [Ando et al. 2015a]). https://ryichando.graphics/download/hindsight_streamfunc.pdf
- Alexis Angelidis and Fabrice Neyret. 2005. Simulation of smoke based on vortex filament primitives. In *Proceedings of the 2005 ACM SIGGRAPH/Eurographics symposium on Computer animation*. 87–96.
- Vladimir I. Arnold. 1966. Sur la géométrie différentielle des groupes de Lie de dimension infinie et ses applications à l'hydrodynamique des fluides parfaits. In *Annales de l'institut Fourier*, Vol. 16. 319–361.
- Vladimir I. Arnold. 1969. On one-dimensional cohomology of the Lie algebra of divergence-free vector fields and on rotation numbers of dynamic systems. In *Vladimir I. Arnold-Collected Works*. Springer, 179–182.
- Vladimir I. Arnold and Boris A. Khesin. 1998. *Topological Methods in Hydrodynamics*. Springer.
- Omri Azencot, Steffen Weißmann, Maks Ovsjanikov, Max Wardetzky, and Mirela Ben-Chen. 2014. Functional fluids on surfaces. In *Computer Graphics Forum*, Vol. 33. Wiley Online Library, 237–246.
- Augustin Banyaga. 1978. Sur la structure du groupe des difféomorphismes qui préservent une forme symplectique. *Commentarii Mathematici Helvetici* 53, 1 (1978), 174–227.
- Ayan Biswas, Richard Strelitz, Jonathan Woodring, Chun-Ming Chen, and Han-Wei Shen. 2016. A scalable streamline generation algorithm via flux-based isocontour extraction. In *Proceedings of the 16th Eurographics Symposium on Parallel Graphics and Visualization*. 69–78.
- Stefanella Boatto and Jair Koeller. 2015. Vortices on closed surfaces. In *Geometry, mechanics, and dynamics*. Springer, 185–237.
- Alain Bossavit. 1998. *Computational Electromagnetism*. Academic Press. <https://www.sciencedirect.com/science/article/pii/B9780121187101500015>
- Robert Bridson. 2015. *Fluid simulation for computer graphics* (2 ed.). CRC press.
- Robert Bridson, Jim Houriham, and Marcus Nordenstam. 2007. Curl-noise for procedural fluid flow. *ACM Transactions on Graphics (TOG)* 26, 3 (2007), 46–es.
- Tyson Brochu, Todd Keeler, and Robert Bridson. 2012. Linear-time smoke animation with vortex sheet meshes. In *Proceedings of the ACM SIGGRAPH/Eurographics Symposium on Computer Animation*. Citeseer, 87–95.
- Jumyung Chang, Vinicius C. Azevedo, and Christopher Batty. 2019. Divergence-Free and Boundary-Respecting Velocity Interpolation Using Stream Functions. In *Proceedings of the 18th Annual ACM SIGGRAPH/Eurographics Symposium on Computer Animation (Los Angeles, California) (SCA '19)*. Association for Computing Machinery, New York, NY, USA, 7:1–7:2. <https://doi.org/10.1145/3309486.3339890>
- Jumyung Chang, Ruben Partono, Vinicius C Azevedo, and Christopher Batty. 2022. Curl-Flow: Boundary-Respecting Pointwise Incompressible Velocity Interpolation for Grid-Based Fluids. *ACM Transactions on Graphics (TOG)* 41, 6 (2022), 243:1–243:21.
- Albert Chern, Felix Knöppel, Ulrich Pinkall, Peter Schröder, and Steffen Weißmann. 2016. Schrödinger's smoke. *ACM Transactions on Graphics (TOG)* 35, 4 (2016), 77:1–77:13.
- Alexandre Joel Chorin and Jerrold E Marsden. 1990. *A mathematical introduction to fluid mechanics*. Vol. 168. Springer.

- Qiaodong Cui, Timothy Langlois, Pradeep Sen, and Theodore Kim. 2021. Spiral-spectral fluid simulation. *ACM Transactions on Graphics (TOG)* 40, 6 (2021), 202:1–202:16.
- Tyler De Witt, Christian Lessig, and Eugene Fiume. 2012. Fluid simulation using laplacian eigenfunctions. *ACM Transactions on Graphics (TOG)* 31, 1 (2012), 10:1–10:11.
- Paweł Dlotko. 2012. A Fast Algorithm to Compute Cohomology Group Generators of Orientable 2-Manifolds. *Pattern Recogn. Lett.* 33, 11 (2012), 1468–1476. <https://doi.org/10.1016/j.patrec.2011.10.005>
- Weinan E and Jian-Guo Liu. 1996. Vorticity boundary condition and related issues for finite difference schemes. *Journal of computational physics* 124, 2 (1996), 368–382.
- Sharif Elcott, Yiyong Tong, Eva Kanso, Peter Schröder, and Mathieu Desbrun. 2007. Stable, circulation-preserving, simplicial fluids. *ACM Transactions on Graphics (TOG)* 26, 1 (2007), 4–es.
- David Eppstein. 2003. Dynamic Generators of Topologically Embedded Graphs. In *Proceedings of the Fourteenth Annual ACM-SIAM Symposium on Discrete Algorithms* (Baltimore, Maryland) (SODA '03). Society for Industrial and Applied Mathematics, USA, 599–608.
- Jeff Erickson and Kim Whittlesey. 2005. Greedy Optimal Homotopy and Homology Generators. In *Proceedings of the Sixteenth Annual ACM-SIAM Symposium on Discrete Algorithms* (Vancouver, British Columbia) (SODA '05). Society for Industrial and Applied Mathematics, USA, 1038–1046.
- Manuel Noronha Gamito, Pedro Faria Lopes, and Mário Rui Gomes. 1995. Two-dimensional simulation of gaseous phenomena using vortex particles. In *Computer Animation and Simulation '95*. Springer, 3–15.
- JS Godfrey. 1989. A Sverdrup model of the depth-integrated flow for the world ocean allowing for island circulations. *Geophysical & Astrophysical Fluid Dynamics* 45, 1-2 (1989), 89–112.
- Abhinav Golas, Rahul Narain, Jason Sewall, Pavel Krajcevski, Pradeep Dubey, and Ming Lin. 2012. Large-scale fluid simulation using velocity-vorticity domain decomposition. *ACM Transactions on Graphics (TOG)* 31, 6 (2012), 148:1–148:9.
- Francis H Harlow and J Eddie Welch. 1965. Numerical calculation of time-dependent viscous incompressible flow of fluid with free surface. *The physics of fluids* 8, 12 (1965), 2182–2189.
- A. Hatcher. 2002. *Algebraic Topology*. Cambridge University Press.
- Anil Nirmal Hirani. 2003. *Discrete exterior calculus*. California Institute of Technology.
- Weizhen Huang, Julian Iseringhausen, Tom Kneiphof, Ziyin Qu, Chenfanfu Jiang, and Matthias B Hullin. 2020. Chemomechanical simulation of soap film flow on spherical bubbles. *ACM Transactions on Graphics (TOG)* 39, 4 (2020), 41:1–41:13.
- Sadashige Ishida, Peter Synak, Fumiya Narita, Toshiya Hachisuka, and Chris Wojtan. 2020. A model for soap film dynamics with evolving thickness. *ACM Transactions on Graphics (TOG)* 39, 4 (2020), 31:1–31:11.
- Sadashige Ishida, Chris Wojtan, and Albert Chern. 2022. Hidden Degrees of Freedom in Implicit Vortex Filaments. *ACM Transactions on Graphics (TOG)* 41, 6 (2022), 24:1–24:12.
- BA Khesin and Yu V Chekanov. 1989. Invariants of the Euler equations for ideal or barotropic hydrodynamics and superconductivity in D dimensions. *Physica D: Nonlinear Phenomena* 40, 1 (1989), 119–131.
- Boris Khesin, Daniel Peralta-Salas, and Cheng Yang. 2022. The helicity uniqueness conjecture in 3D hydrodynamics. *Trans. Amer. Math. Soc.* 375, 02 (2022), 909–924.
- ByungMoon Kim, Yingjie Liu, Ignacio Llamas, and Jaroslav R Rossignac. 2005. *Flowfixer: Using BFEC for fluid simulation*. Technical Report. Georgia Institute of Technology.
- John M Lee. 2013. Smooth manifolds. In *Introduction to smooth manifolds*. Springer, 1–31.
- CC Lin. 1941. On the motion of vortices in two dimensions: I. Existence of the Kirchhoff-Routh function. *Proceedings of the National Academy of Sciences* 27, 12 (1941), 570–575.
- Beibei Liu, Gemma Mason, Julian Hodgson, Yiyong Tong, and Mathieu Desbrun. 2015. Model-reduced variational fluid simulation. *ACM Transactions on Graphics (TOG)* 34, 6 (2015), 244:1–244:12.
- Jerrold Marsden and Alan Weinstein. 1983. Coadjoint Orbits, Vortices, and Clebsch Variables for Incompressible Fluids. *Physica D: Nonlinear Phenomena* 7, 1 (1983), 305–323.
- Akira Mizukami. 1983. A stream function-vorticity finite element formulation for Navier-Stokes equations in multi-connected domain. *International journal for numerical methods in engineering* 19, 9 (1983), 1403–1409.
- Philip J Morrison. 1998. Hamiltonian description of the ideal fluid. *Reviews of modern physics* 70, 2 (1998), 467.
- Mohammad Sina Nabizadeh, Stephanie Wang, Ravi Ramamoorthi, and Albert Chern. 2022. Covector fluids. *ACM Transactions on Graphics (TOG)* 41, 4 (2022), 113:1–113:16.
- Steven A Orszag and Moshe Israeli. 1974. Numerical simulation of viscous incompressible flows. *Annual Review of Fluid Mechanics* 6, 1 (1974), 281–318.
- VI Oseledets. 1989. On a new way of writing the Navier-Stokes equation. The Hamiltonian formalism. *Russ. Math. Surveys* 44 (1989), 210–211.
- Marcel Padilla. 2018. Point vortex dynamics on closed surfaces. *Master thesis, Technische Universität Berlin* (2018).
- David Palmer, Dmitriy Smirnov, Stephanie Wang, Albert Chern, and Justin Solomon. 2022. DeepCurrents: Learning Implicit Representations of Shapes with Boundaries. *Proceedings of the IEEE/CVF Conference on Computer Vision and Pattern Recognition (CVPR)* (2022).
- Sang Il Park and Myoung Jun Kim. 2005. Vortex fluid for gaseous phenomena. In *Proceedings of the 2005 ACM SIGGRAPH/Eurographics symposium on Computer animation*. 261–270.
- Dmitry Pavlov, Patrick Mullen, Yiyong Tong, Eva Kanso, Jerrold E Marsden, and Mathieu Desbrun. 2011. Structure-preserving discretization of incompressible fluids. *Physica D: Nonlinear Phenomena* 240, 6 (2011), 443–458.
- Joseph Pedlosky, Lawrence J Pratt, Michael A Spall, and Karl R Helfrich. 1997. Circulation around islands and ridges. *Journal of Marine Research* 55, 6 (1997), 1199–1251.
- Konstantin Poelke and Konrad Polthier. 2016. Boundary-aware Hodge decompositions for piecewise constant vector fields. *Computer-Aided Design* 78 (2016), 126–136.
- Luigi Quartapelle. 1993. *Numerical solution of the incompressible Navier-Stokes equations*. Vol. 113. Springer Science & Business Media.
- L Quartapelle and F Valz-Gris. 1981. Projection conditions on the vorticity in viscous incompressible flows. *International Journal for Numerical Methods in Fluids* 1, 2 (1981), 129–144.
- M Rank and A Voigt. 2021. Active flows on curved surfaces. *Physics of Fluids* 33, 7 (2021), 072110.
- Dietmar Rempfer. 2006. On boundary conditions for incompressible Navier-Stokes problems. *Applied Mechanics Reviews* 59 (2006), Issue 3.
- Damien Rioux-Lavoie, Ryusuke Sugimoto, Tümay Özdemir, Naoharu H. Shimada, Christopher Batty, Derek Nowrouzezahrai, and Toshiya Hachisuka. 2022. A Monte Carlo Method for Fluid Simulation. *ACM Transactions on Graphics (TOG)* 41, 6 (2022), 240:1–240:16.
- Rick Salmon. 1988. Hamiltonian fluid mechanics. *Annual review of fluid mechanics* 20, 1 (1988), 225–256.
- Syuhei Sato, Yoshinori Dobashi, Kei Iwasaki, Tsuyoshi Yamamoto, and Tomoyuki Nishita. 2014. Deformation of 2D Flow Fields Using Stream Functions. In *SIGGRAPH Asia 2014 Technical Briefs* (Shenzhen, China) (SA '14). Association for Computing Machinery, New York, NY, USA, 4:1–4:4.
- Syuhei Sato, Yoshinori Dobashi, and Theodore Kim. 2021. Stream-Guided Smoke Simulations. *ACM Transactions on Graphics (TOG)* 40, 4 (2021), 161:1–161:7.
- Günter Schwarz. 2006. *Hodge Decomposition-A method for solving boundary value problems*. Springer.
- Andrew Selle, Ronald Fedkiw, Byungmoon Kim, Yingjie Liu, and Jarek Rossignac. 2008. An unconditionally stable MacCormack method. *Journal of Scientific Computing* 35, 2 (2008), 350–371.
- Lin Shi and Yizhou Yu. 2004. Inviscid and incompressible fluid simulation on triangle meshes. *Computer Animation and Virtual Worlds* 15, 3-4 (2004), 173–181.
- Clayton Shonkwiler. 2009. *Poincaré duality angles on Riemannian manifolds with boundary*. Ph. D. Dissertation. University of Pennsylvania.
- Yousuf Soliman, Albert Chern, Olga Diamanti, Felix Knöppel, Ulrich Pinkall, and Peter Schröder. 2021. Constrained Willmore surfaces. *ACM Transactions on Graphics (TOG)* 40, 4 (2021), 112:1–112:17.
- Jos Stam. 2003. Flows on surfaces of arbitrary topology. *ACM Transactions on Graphics (TOG)* 22, 3 (2003), 724–731.
- Cedric Taylor and Paul Hood. 1973. A numerical solution of the Navier-Stokes equations using the finite element technique. *Computers & Fluids* 1, 1 (1973), 73–100.
- Tayfun E Tezduyar, Roland Glowinski, and J Liou. 1988. Petrov-Galerkin methods on multiply connected domains for the vorticity-stream function formulation of the incompressible Navier-Stokes equations. *International journal for numerical methods in fluids* 8, 10 (1988), 1269–1290.
- Alexander Thom. 1933. The flow past circular cylinders at low speeds. *Proceedings of the Royal Society of London. Series A, Containing Papers of a Mathematical and Physical Character* 141, 845 (1933), 651–669.
- William Thomson. 1868. On Vortex Motion. *Earth and Environmental Science Transactions of the Royal Society of Edinburgh* 25, 1 (1868), 217–260.
- Joris Vankerschaver, Eva Kanso, and Jerrold E Marsden. 2009. The geometry and dynamics of interacting rigid bodies and point vortices. *Journal of Geometric Mechanics* 1, 2 (2009), 223–266.
- Mauricio Vines, Ben Houston, Jochen Lang, and Won-Sook Lee. 2013. Vortical inviscid flows with two-way solid-fluid coupling. *IEEE Transactions on Visualization and Computer Graphics* 20, 2 (2013), 303–315.
- Stephanie Wang and Albert Chern. 2021. Computing Minimal Surfaces with Differential Forms. *ACM Transactions on Graphics (TOG)* 40, 4 (2021), 113:1–113:14.
- Alan Weinstein. 1998. Poisson geometry. *Differential Geometry and its applications* 9, 1-2 (1998), 213–238.
- Steffen Weißmann. 2014. Hamiltonian dynamics of several rigid bodies interacting with point vortices. *Journal of Nonlinear Science* 24 (2014), 359–382.
- Steffen Weißmann and Ulrich Pinkall. 2010. Filament-Based Smoke with Vortex Shedding and Variational Reconnection. *ACM Transactions on Graphics (TOG)* 29, 4 (2010), 115:1–115:12.
- Steffen Weißmann and Ulrich Pinkall. 2012. Underwater rigid body dynamics. *ACM Transactions on Graphics (TOG)* 31, 4 (2012), 104:1–104:7.

- Shiyong Xiong, Rui Tao, Yaorui Zhang, Fan Feng, and Bo Zhu. 2021. Incompressible Flow Simulation on Vortex Segment Clouds. *ACM Transactions on Graphics (TOG)* 40, 4 (2021), 98:1–98:11.
- Larry Yaeger, Craig Upson, and Robert Myers. 1986. Combining Physical and Visual Simulation—Creation of the Planet Jupiter for the Film “2010” (*SIGGRAPH ’86*). Association for Computing Machinery, New York, NY, USA, 85–93.
- Shuqi Yang, Shiyong Xiong, Yaorui Zhang, Fan Feng, Jinyuan Liu, and Bo Zhu. 2021. Clebsch gauge fluid. *ACM Transactions on Graphics (TOG)* 40, 4 (2021), 99:1–99:11.
- Xinxin Zhang and Robert Bridson. 2014. A PPPM fast summation method for fluids and beyond. *ACM Transactions on Graphics (TOG)* 33, 6 (2014), 206:1–206:11.
- Xinxin Zhang, Robert Bridson, and Chen Greif. 2015. Restoring the missing vorticity in advection-projection fluid solvers. *ACM Transactions on Graphics (TOG)* 34, 4 (2015), 52:1–52:8.
- Rundong Zhao, Mathieu Desbrun, Guo-Wei Wei, and Yiyong Tong. 2019. 3D Hodge decompositions of edge-and face-based vector fields. *ACM Transactions on Graphics (TOG)* 38, 6 (2019), 181:1–181:13.

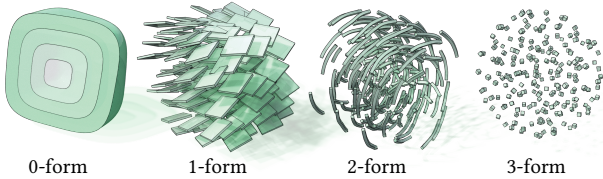
A PRELIMINARIES

A.1 Differential Forms

Let M be an n -dimensional Riemannian manifold. The space of vector fields is denoted by $\Gamma(TM)$, and the space of differential k -forms, $0 \leq k \leq n$, is denoted by $\Omega^k(M)$.

A differential k -form $\alpha \in \Omega^k(M)$ is a formal object to-be-integrated over an oriented k -dimensional test surface S . This evaluation method is denoted by $\int_S \alpha$. For example, in 3D, a 3-form describes a density field or a measure that awaits being integrated over a volumetric region. A 2-form describes a flux that is to be evaluated over an oriented surface. A 1-form is to be line-integrated into circulations, and 0-forms are synonyms for scalar functions that are to be evaluated over points.

A.1.1 Forms are Distributions of Codimensional Geometries. Differential k -forms should not be confused with vector fields in their visual representations. Geometrically, a vector field \mathbf{v} is an assignment of an infinitesimal “arrow” $\mathbf{v}_p \in T_p M$ at every point $p \in M$, whose directions and magnitudes depict an instantaneous flow velocity within the domain M . A k -form $\alpha \in \Omega^k(M)$, on the other hand, is a distribution of $(n-k)$ -dimensional (codimension- k) oriented planes over M . For example, in 3D, a 3-form is illustrated as a point cloud, a 2-form is a line segment cloud, a 1-form is a plane field, and a 0-form is a superposition of sublevel sets of the corresponding scalar function. The orientations and densities of the codimension- k plane cloud are given so that the integration $\int_S \alpha$ over a test k -surface S is the total signed intersection between S and the codimensional- k plane cloud.¹¹

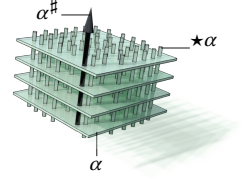


A.1.2 Type Conversions. The Riemannian metric over the manifold defines a notion of distance and orthogonality. The magnitude $|\alpha|$ of a k -form α is the throughput of the codimension cloud across an orthogonal cross section of unit k -area. The Hodge star converts

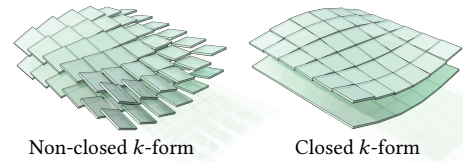
¹¹For $n = 2, 3$, every k -form at each tangent space admits a distinguished $(n-k)$ -subspace that represents the orientation of the plane field. For $n > 3$ and $1 < k < n-1$, the codimension- k plane fields are generally no longer described by a distinguished oriented subspace but a superposition of many.

a k -form to a $(n-k)$ -form, $\star: \Omega^k(M) \rightarrow \Omega^{n-k}(M)$, so that the codimension cloud of $\star\alpha$ is pointwise the orthogonal complement of the codimension cloud of α , and that they share the same magnitude $|\star\alpha| = |\alpha|$. The parity is chosen so that $\star\star\alpha = (-1)^{k(n-k)}\alpha$ for a k -form α .

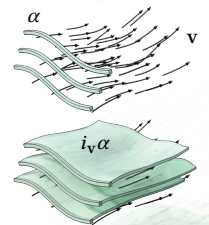
A 1-form can be converted into a vector, and vice versa, by the sharp $\sharp: \Omega^1(M) \rightarrow \Gamma(TM)$ and flat $\flat = \sharp^{-1}: \Gamma(TM) \rightarrow \Omega^1(M)$ operators. For a 1-form $\alpha \in \Omega^1(M)$, the vector field α^\sharp is pointwise an arrow whose direction is orthogonal to the hyperplane of α at the point, and whose magnitude is set as $|\alpha^\sharp| = |\alpha|$. An $(n-1)$ -form β (typically representing a flux) can also be converted into a vector by $(\star\beta)^\sharp$. Both 1-forms and $(n-1)$ -forms are often identified as vector fields; α^\sharp is a vector field orthogonal to the hyperplane field $\alpha \in \Omega^1(M)$, and $(\star\beta)^\sharp$ is a vector tangential to the line field $\beta \in \Omega^{n-1}(M)$. See also Tables 1 and 2.



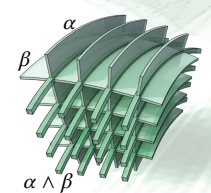
A.1.3 Exterior Derivatives are Boundary Operators. The exterior derivative operator $d: \Omega^k(M) \rightarrow \Omega^{k+1}(M)$ takes the boundary of the codimensional geometric representation. For each $\alpha \in \Omega^k(M)$, its exterior derivative $d\alpha \in \Omega^{k+1}(M)$ has the $(n-k-1)$ dimensional cloud elements given by the boundaries of the $(n-k)$ -dimensional cloud elements of α . The Stokes Theorem $\int_S d\alpha = \oint_{\partial S} \alpha$ can be interpreted as the invariant of intersection number when swapping the boundary operation. A k -form $\alpha \in \Omega^k(M)$ is closed if $d\alpha = 0$. For a closed form, the boundaries of each instance of the codimensional cloud cancel out with the neighboring boundaries. As a consequence, the codimensional cloud of a closed form stitches together into global pieces of $(n-k)$ -dimensional surfaces foliating the space.



A.1.4 Interior Products are Extrusions. The interior product $i_v \alpha$ of a k -form $\alpha \in \Omega^k$ with a vector field $\mathbf{v} \in \Gamma(TM)$ is a $(k-1)$ -form whose codimension cloud is given by the extrusion of the codimension cloud of α along \mathbf{v} .



A.1.5 Wedge Products are Intersections. The wedge product $\alpha \wedge \beta$ of a k -form $\alpha \in \Omega^k(M)$ and an ℓ -form $\beta \in \Omega^\ell(M)$ is a $(k+\ell)$ -form whose codimension cloud is given by the intersection of the codimension clouds of α and β .



A.1.6 Lie Derivatives and Advections of the Codimension Cloud. A time varying k -form $\alpha \in \Omega^k(M)$ is said to be advected by a velocity field $\mathbf{v} \in \Gamma(TM)$ if its codimension cloud is passively transported and deformed by the flow generated by \mathbf{v} . The corresponding advection equation is given by $\frac{\partial \alpha}{\partial t} + \mathcal{L}_v \alpha = 0$ where $\mathcal{L}_v \alpha \in \Omega^k(M)$ is the Lie

derivative of α with respect to \mathbf{v} . Using geometric pictures relating advection and extrusion along a flow, one finds $\mathcal{L}_V \alpha = \text{div}_V \alpha + i_V d\alpha$:

$$(61)$$

known as the *Cartan formula*. Note that the green and white shades represent the orientations. For a general time-dependent k -form α , the *Lie material derivative* $\frac{\partial \alpha}{\partial t} + \mathcal{L}_V \alpha$ measures the rate of change of α following the flow.

A.1.7 Dirac δ -Forms. A Dirac δ -form, also known as an *integral current* [Wang and Chern 2021; Palmer et al. 2022], is a differential form whose codimension cloud is concentrated to a single geometry. For a codimension- k surface $\Gamma \subset M$, the associated Dirac- δ form $\delta_\Gamma \in \Omega^k(M)$ is a k -form such that $\int_M \beta \wedge \delta_\Gamma = \int_\Gamma \beta$ for all $\beta \in \Omega^{n-k}(M)$. Equivalently, $\int_S \delta_\Gamma$ is the signed intersection between Γ and any k -dimensional test surface S . For codimension- k surface Γ and codimension- ℓ surface Σ , we have $d\delta_\Gamma = (-1)^{k+1} \delta_{\partial\Gamma}$ and $\delta_\Gamma \wedge \delta_\Sigma = \delta_{\Gamma \cap \Sigma}$.

A.1.8 Dirichlet Data are Intersections with Boundary. Suppose the domain M has a boundary ∂M . Let $j: \partial M \hookrightarrow M$ denote the inclusion map. For each k -form $\alpha \in \Omega^k(M)$, we call the pullback $j^* \alpha \in \Omega^k(\partial M)$ of α by j the *Dirichlet boundary data* of α . Geometrically, the codimension- k cloud for $j^* \alpha$, which is $(n-1-k)$ -dimensional elements within the $(n-1)$ -dimensional ∂M , is given by the intersection of ∂M with the codimension cloud of α .

A.1.9 Dirichlet and Co-Dirichlet Boundary Conditions. A k -form $\alpha \in \Omega^k(M)$ is said to be *Dirichlet* if $j^* \alpha = 0$. It is said to be *co-Dirichlet* if $j^* \star \alpha = 0$. Under the Dirichlet boundary (resp. co-Dirichlet boundary) condition, the codimensional geometry is tangential (resp. normal) to the boundary. See Tables 1 and 2 for these boundary conditions in terms of the scalar and vector notations.

A.1.10 L^2 Inner Products and Codifferentials. The L^2 inner product between two k -forms $\alpha, \beta \in \Omega^k(M)$ is denoted and given by $\langle\langle \alpha, \beta \rangle\rangle = \int_M \alpha \wedge \star \beta$. The codifferential $\delta \alpha \in \Omega^{k-1}(M)$ of a k -form α is defined by $\delta \alpha = (-1)^k \star^{-1} d \star \alpha$. Up to a boundary term, the codifferential $\delta: \Omega^{k+1}(M) \rightarrow \Omega^k(M)$ is the adjoint of d with respect to the L^2 inner product using Green's Identity

$$\langle\langle d\gamma, \sigma \rangle\rangle = \langle\langle \gamma, \delta \sigma \rangle\rangle + \oint_{\partial M} (j^* \gamma) \wedge (j^* \star \sigma) \quad (62)$$

which holds for all $\gamma \in \Omega^k(M)$ and $\sigma \in \Omega^{k+1}(M)$.

A.2 Homology Theory

We review the definitions and the notations in the (singular) homology theory. Let M be a smooth manifold with boundary $j: \partial M \hookrightarrow M$. A *k -chain* is a formal linear combination of k -dimensional primitive geometries in M . Concretely, each primitive k -dimensional geometry is a smooth map that places a k -dimensional simplex into M . The notion of boundary of a k -chain is inherited from the notion of boundary of a simplex.

A.2.1 Absolute Homology. The linear space of k -chains in M is denoted by $C_k(M)$. The boundary operator is a linear map $\partial_k: C_k(M) \rightarrow C_{k-1}(M)$ given by its definition on each primitive geometry. The boundary operators satisfy $\partial_{k-1} \circ \partial_k = 0$. A k -chain $\Gamma \in C_k(M)$ is said to be *closed*, or a *cycle*, if $\partial_k \Gamma = 0$. A k -chain $\Gamma \in C_k(M)$ is called *exact*, or a *boundary*, if $\Gamma = \partial_{k+1} \Sigma$ for some $(k+1)$ -chain $\Sigma \in C_{k+1}(M)$. The subspace of k -cycles and k -boundaries are respectively denoted by

$$Z_k(M) := \ker(\partial_k) \subset C_k(M), \quad (63)$$

$$B_k(M) := \text{im}(\partial_{k+1}) \subset Z_k(M) \subset C_k(M). \quad (64)$$

Two cycles $\Gamma_1, \Gamma_2 \in Z_k(M)$ are said to be *homologous* if $\Gamma_1 - \Gamma_2 \in B_k(M)$; that is, Γ_1, Γ_2 *coborder* a $(k+1)$ -chain. The *k -th homology* is the collection of “types” (equivalence classes) of cycles after identifying homologous cycles. Algebraically, the k -th homology is defined by the quotient space

$$H_k(M) := Z_k(M)/B_k(M). \quad (65)$$

A.2.2 Relative Homology. The general idea of homology theory relative to ∂M is to allow cycles to have boundaries attached to ∂M . The algebraic trick for regarding these geometries as cycles is to “ignore ∂M .”

Define the space of *relative k -chains* by

$$C_k(M, \partial M) := C_k(M)/C_k(\partial M). \quad (66)$$

That is, two k -chains represent the same object in $C_k(M, \partial M)$ if they differ only on ∂M . One may verify that the boundary operator ∂_k is well-defined on $C_k(M, \partial M)$. Hence we have $\partial_k: C_k(M, \partial M) \rightarrow C_{k-1}(M, \partial M)$ satisfying the same structural equation $\partial_{k-1} \circ \partial_k = 0$. Analogous to the absolute homology theory, one defines the spaces of *relative cycles* and *relative boundaries* respectively by

$$Z_k(M, \partial M) := \ker(\partial_k) \subset C_k(M, \partial M) \quad (67)$$

$$B_k(M, \partial M) := \text{im}(\partial_{k+1}) \subset Z_k(M, \partial M) \subset C_k(M, \partial M). \quad (68)$$

A representative of a relative cycle may have a boundary that is contained in ∂M . Two relative cycles Γ_1, Γ_2 are *homologous* if $\Gamma_1 - \Gamma_2$ is the boundary of some Σ modulo ∂M . The *k -th relative homology*

$$H_k(M, \partial M) := Z_k(M, \partial M)/B_k(M, \partial M) \quad (69)$$

is the collection of types of relative cycles after the identification of homologous cycles.

B POISSON PROBLEM FOR STREAM FORM

In this appendix, we describe the system of equations one needs to solve for constructing $d^+ \omega \in \Omega^k(M)$ for a $(k+1)$ -form $\omega \in \text{im}(d) \subset \Omega^{k+1}(M)$.

By Proposition 4, we know that $d^+ \omega$ takes the form of

$$d^+ \omega = \delta \psi \quad \text{for some } \psi \in \Omega^{k+1}(M), j^* \star \psi = 0. \quad (70)$$

This stream form ψ is not unique by additive factors of $\ker(\delta)$.

Definition 6 (Coulomb gauge). *The particular solution ψ to (70) is said to satisfy the Coulomb gauge if $d\psi = 0$ and $\psi \perp \mathcal{H}_C^{k+1}(M)$.*

Proposition 10. *The Coulomb gauge solution ψ to (70) is the unique solution to the boundary-value Poisson problem*

$$\begin{cases} (d\delta + \delta d)\psi = \omega & \text{in } M, \\ j^* \star \psi = 0 & \text{on } \partial M, \\ j^* \star d\psi = 0 & \text{on } \partial M, \\ \psi \perp \mathcal{H}_C^{k+1}(M). \end{cases} \quad \begin{array}{l} (71a) \\ (71b) \\ (71c) \\ (71d) \end{array}$$

PROOF. By the invertibility of d, d^+ between $\text{im}(d)$ and $\text{im}(d^+)$ (Proposition 3), (70) is equivalent to

$$d\delta\psi = \omega, \quad j^* \star \psi = 0. \quad (72)$$

The addition of the Coulomb gauge conditions (especially $d\psi = 0$) ensures (71a) and (71c). Conversely, suppose ψ solves (71).¹² We only need to show $d\psi = 0$; if so, then (72) and the rest of the Coulomb conditions follow. To show $d\psi = 0$, apply d on both sides of (71a) to obtain $d\delta d\psi = 0$. This equation implies $\|\delta d\psi\|^2 = \langle \delta d\psi, \delta d\psi \rangle = \langle d\delta d\psi, d\psi \rangle = 0$ by (62) and (71c). Therefore, $\delta d\psi = 0$. This once again implies $\langle d\psi, d\psi \rangle = \langle \psi, \delta d\psi \rangle = 0$ using (62) and (71b). Hence $d\psi = 0$, which completes the proof. \square

Remark 7. *The condition (71d) in the Coulomb gauge ensures the uniqueness of (71). In practice, the condition (71d) is sometimes neither mentioned nor enforced. This is fine, as the remaining system of (71) only has a small finite dimensional kernel of $\mathcal{H}_C^{k+1}(M)$, which does not jeopardize most linear solvers and does not influence the result of $\delta\psi$ in (70).*

B.1 Solving Streamfunctions in 2D

In 2D, the stream form $\psi \in \Omega^2(M)$ is a top-degree form, and therefore (71c) drops. With the both the vorticity 2-form ω and the stream form ψ written as their scalar counterparts $w, \hat{\psi}$ ($\omega = \star w, \psi = \star \hat{\psi}$), Eq. (71) becomes a Dirichlet value problem:

$$\begin{cases} -\Delta \hat{\psi} = w, \\ \hat{\psi}|_{\partial M} = 0, \\ \hat{\psi} \perp \mathcal{H}_D^0(M), \end{cases} \quad \begin{array}{l} (73a) \\ (73b) \\ (73c) \end{array}$$

where $-\Delta = \delta d$ is the scalar Laplacian. On a connected domain M without boundary, we have $\mathcal{H}_D^0(M) = \{\text{constant functions}\} \cong \mathbb{R}$. In that case, (73b) drops, and (73c) reads as a zero-mean condition $\int_M \hat{\psi} dA = 0$. If M has boundary, then $\mathcal{H}_D^0(M) = \{0\}$, and the condition (73c) drops.

On a triangle mesh, we set both w and $\hat{\psi}$ on vertices following [Azencot et al. 2014]. Another possible approach is to let the values of w and $\hat{\psi}$ sit on edge centers, and represent $\hat{\psi}$ using the Crouzeix-Raviart elements [Poelke and Polthier 2016].

B.2 Solving Streamfunctions on a 3D MAC Grid

Here, we describe an implementation of (71) in 3D under the Marker-And-Cell (MAC) discretization scheme [Harlow and Welch 1965; Bridson 2015]. The streamfunction solve is a simplified special case of [Ando et al. 2015a] without a varying density. In the MAC scheme, the velocity field is given as fluxes assigned to the faces on a regular grid. The vorticity and the streamfunction are defined on edges. That

¹²The existence and the uniqueness for the solution to (71) is given by [Schwarz 2006, Corollary 3.4.8].

is, the MAC scheme is equivalent to a Discrete Exterior Calculus (DEC) scheme for our exterior calculus formulation up to a Hodge dual. For notation distinction, let $\hat{\eta} = \star \eta \in \Omega^2(M)$ be the velocity flux defined on faces, $\hat{\omega} = \star \omega \in \Omega^1(M)$ be the vorticity 1-form defined on edges, and $\hat{\psi} = \star \psi$ be the stream 1-form on edges.

Let the grid (V, E, F, C) be organized by the vertex set V , edge set E , face set F and cell set C . We assume every edge has length h . The adjacency and orientation between the cubical complex are summarized in the discrete exterior derivative matrices (a.k.a. *coboundary operators*) forming a (co)chain complex

$$\mathbb{R}^{|V|} \xrightarrow{d_0} \mathbb{R}^{|E|} \xrightarrow{d_1} \mathbb{R}^{|F|} \xrightarrow{d_2} \mathbb{R}^{|C|}, \quad d_1 d_0 = 0, \quad d_2 d_1 = 0. \quad (74)$$

Note that each matrix d_k has entries either $-1, 0, 1$. The division by h in a finite difference derivative will be denoted separately, keeping d_k 's purely topological.

To assign obstacles, for each cell in C , label ‘‘fluid (interior I)’’ or ‘‘solid (boundary B).’’ Next, label fluid and solid on V, E, F by taking *the closure of the solid cells*. That is, first initialize each element of V, E, F as fluid, and then label every boundary face of a solid cell a ‘‘solid’’ face; subsequently, label every boundary edge of every solid face as solid, and finally label every boundary vertex of every boundary edge as solid. After consistently labeling of fluid (I) and solid (B) elements $V = V_I \sqcup V_B, E = E_I \sqcup E_B, F = F_I \sqcup F_B, C = C_I \sqcup C_B$, slice the coboundary operators into

$$d_1 = \begin{array}{c|cc} & |E_I| & |E_B| \\ \hline |F_I| & d_{1,II} & d_{1,IB} \\ \hline |F_B| & \mathbf{0} & d_{1,BB} \end{array} : \mathbb{R}^{|E_I|} \oplus \mathbb{R}^{|E_B|} \rightarrow \mathbb{R}^{|F_I|} \oplus \mathbb{R}^{|F_B|} \quad (75)$$

and similarly for the other d_k 's. One checks that the interior (fluid) blocks form a cochain complex:

$$\mathbb{R}^{|V_I|} \xrightarrow{d_{0,II}} \mathbb{R}^{|E_I|} \xrightarrow{d_{1,II}} \mathbb{R}^{|F_I|} \xrightarrow{d_{2,II}} \mathbb{R}^{|C_I|}, \quad d_{k+1,II} d_{k,II} = \mathbf{0}, \quad (76)$$

which is known as the relative cochain complex.

Now, the no-through boundary condition $j^* \hat{\eta} = 0$ and the Dirichlet condition $j^* \hat{\psi} = 0$ translates to the fact that $\hat{\eta}$ and $\hat{\psi}$ only live on F_I and E_I respectively, and vanish over F_B, E_B . The discrete relation between the streamfunction $\hat{\psi} \in \mathbb{R}^{|E_I|}$ and $\hat{\eta} \in \mathbb{R}^{|F_I|}$ is given by

$$\hat{\eta} = \frac{1}{h} d_{1,II} \hat{\psi}. \quad (77)$$

Take ‘‘curl’’ $\frac{1}{h} d_{1,II}^T$ on both sides of the equation:

$$\hat{\omega}_I = \frac{1}{h} d_{1,II}^T \hat{\eta} = \frac{1}{h^2} d_{1,II}^T d_{1,II} \hat{\psi}. \quad (78)$$

We label $\hat{\omega}_I \in \mathbb{R}^{|E_I|}$ with subscript I to acknowledge that $\hat{\omega}_B = \frac{1}{h} d_{1,IB}^T \hat{\eta}$ does not need to be zero. However, we will see $\hat{\omega}_B \in \mathbb{R}^{|E_B|}$ do not play a role in determining $\hat{\psi} \in \mathbb{R}^{|E_I|}$.

Given interior vorticity data $\hat{\omega}_I \in \mathbb{R}^{|E_I|}$, we solve a particular solution $\hat{\psi}$ to (78) by the linear system

$$\underbrace{\frac{1}{h^2} (d_{1,II}^T d_{1,II} + d_{0,II} d_{0,II}^T)}_{=:L} \hat{\psi} = \hat{\omega}_I. \quad (79)$$

Proposition 11. *Any solution $\hat{\psi} \in \mathbb{R}^{|E_I|}$ to (79) satisfies (78) and a Coulomb gauge condition $d_{0,II}^T \hat{\psi} = \mathbf{0}$.*

PROOF. It suffices to show that any solution to (79) satisfies $\mathbf{d}_{0,II}^\top \hat{\psi} = \mathbf{0}$. Apply $\mathbf{d}_{0,II}^\top$ on (79) to obtain $\mathbf{d}_{0,II}^\top \mathbf{d}_{0,II} \mathbf{d}_{0,II}^\top \hat{\psi} = \mathbf{0}$ using $\hat{\omega}_I \in \text{im}(\mathbf{d}_{1,II}^\top)$ and (76). This equation ensures that $|\mathbf{d}_{0,II} \mathbf{d}_{0,II}^\top \hat{\psi}|^2 = \hat{\psi}^\top \mathbf{d}_{0,II}^\top \mathbf{d}_{0,II} \mathbf{d}_{0,II}^\top \hat{\psi} = 0$. Therefore, $\mathbf{d}_{0,II} \mathbf{d}_{0,II}^\top \hat{\psi} = \mathbf{0}$. Hence, $|\mathbf{d}_{0,II}^\top \hat{\psi}|^2 = \hat{\psi}^\top \mathbf{d}_{0,II} \mathbf{d}_{0,II}^\top \hat{\psi} = 0$, and thus $\mathbf{d}_{0,II}^\top \hat{\psi} = \mathbf{0}$. \square

C LINKING NUMBER IN GENERAL DOMAIN

Here we provide a well-defined linking number (Theorem 2) between two fields on a general manifold M . This linking number between smooth fields is also called the *cross-helicity*. For general domain, define the linking $\text{LINK}(\omega)(\xi)$ between a closed k -form ω and a closed Dirichlet $(n - k + 1)$ -form ξ by its variation with respect to local transportations $\hat{\omega} = \mathcal{L}_Y \omega$ while fixing ξ :

$$\frac{\delta \text{LINK}(\omega)(\xi)}{\delta \omega} \llbracket \mathcal{L}_Y \omega \rrbracket := \int_M (i_Y \omega) \wedge \xi. \quad (80)$$

Now, we verify this variational gradient is indeed a gradient by checking that the second derivatives commute. Take two vector fields Y_1, Y_2 with Lie commutativity $[Y_1, Y_2] = 0$ (i.e. two coordinate directions on the diffeomorphism group $\text{Diff}(M)$). The mixed second derivative is

$$\frac{\delta}{\delta \omega} \left(\frac{\delta \text{LINK}(\omega)(\xi)}{\delta \omega} \llbracket \mathcal{L}_{Y_1} \omega \rrbracket \right) \llbracket \mathcal{L}_{Y_2} \omega \rrbracket \quad (81)$$

$$= \int_M (i_{Y_1} \mathcal{L}_{Y_2} \omega) \wedge \xi = \int_M (\mathcal{L}_{Y_2} i_{Y_1} \omega - i_{[Y_2, Y_1]} \omega) \wedge \xi \quad (82)$$

$$= \int_M (i_{Y_2} di_{Y_1} \omega + di_{Y_2} i_{Y_1} \omega) \wedge \xi = \int_M (i_{Y_2} \mathcal{L}_{Y_1} \omega) \wedge \xi \quad (83)$$

$$= \frac{\delta}{\delta \omega} \left(\frac{\delta \text{LINK}(\omega)(\xi)}{\delta \omega} \llbracket \mathcal{L}_{Y_2} \omega \rrbracket \right) \llbracket \mathcal{L}_{Y_1} \omega \rrbracket \quad (84)$$

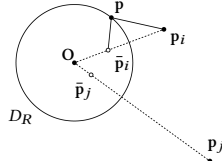
where we have used $d\omega = 0$ and the Dirichlet closedness of ξ for $\int_M d(\cdot) \wedge \xi = 0$ in the second to last equality. Therefore, for each fixed ξ , $\text{LINK}(\omega)(\xi)$ is well-defined locally in the space of ω 's Lie-transported by diffeomorphisms.

D ANALYTICAL EXAMPLE

We demonstrate an analytical example of Corollary 2 by considering point vortices with strengths $\kappa_1, \dots, \kappa_N$ located at $\mathbf{p}_1, \dots, \mathbf{p}_N$ in the plane exterior to a circular obstacle D_R of radius R centered at the origin. Note that \mathbf{p}_i 's move over time while κ_i 's remain constant. Using the method of images, the vortex dynamics can be represented without the obstacle by introducing mirrored vortices reflected in the disk. These mirrored vortices have strengths $\bar{\kappa}_i = -\kappa_i$ and positions $\bar{\mathbf{p}}_i = \frac{R^2}{|\mathbf{p}_i|^2} \mathbf{p}_i$. The domain $\mathbb{R}^2 \setminus D_R$ admits a harmonic vector field given by the clockwise 90° rotated gradient of $U(\mathbf{x}) = \frac{1}{2\pi} \log |\mathbf{x}|$. The corresponding vortex-harmonic streamline linking number is

$$\text{LINK} = \sum_{i=1}^N \kappa_i U(\mathbf{p}_i) = \sum_{i=1}^N \frac{\kappa_i}{2\pi} \log |\mathbf{p}_i|. \quad (85)$$

The flux over any cross-section extending from the obstacle boundary to infinity can be computed by the difference of the streamfunction at the endpoints of the cross-section. In this case, the flux is the negative streamfunction value $-\psi(\mathbf{p}) = -\sum_{i=1}^N (\kappa_i G(\mathbf{p}, \mathbf{p}_i) + \bar{\kappa}_i G(\mathbf{p}, \bar{\mathbf{p}}_i))$ at any $\mathbf{p} \in \partial D_R$, where $G(\mathbf{x}, \mathbf{y}) = -\frac{1}{2\pi} \log |\mathbf{x} - \mathbf{y}|$ is the \mathbb{R}^2 -Green's function. Using the geometric identity that the ratio $|\mathbf{p} - \mathbf{p}_i|/|\mathbf{p} - \bar{\mathbf{p}}_i|$ is



the constant $|\mathbf{p}_i|/R$, we obtain

$$\text{FLUX} = -\psi(\mathbf{p}) = \sum_{i=1}^N \left(\frac{\kappa_i}{2\pi} \log |\mathbf{p} - \mathbf{p}_i| - \frac{\kappa_i}{2\pi} \log |\mathbf{p} - \bar{\mathbf{p}}_i| \right) \quad (86)$$

$$= \sum_{i=1}^N \frac{\kappa_i}{2\pi} \log \frac{|\mathbf{p} - \mathbf{p}_i|}{|\mathbf{p} - \bar{\mathbf{p}}_i|} = \sum_{i=1}^N \frac{\kappa_i}{2\pi} \log \frac{|\mathbf{p}_i|}{R}. \quad (87)$$

In particular, we find that

$$\text{FLUX} - \text{LINK} = -\log R \left(\sum_{i=1}^N \kappa_i \right), \quad (88)$$

which is indeed constant over time.

E PROOFS

E.1 Proof of Proposition 1

To prove $\text{im}(d)^\perp = \mathcal{V}^k$, we show that $\langle\langle d\alpha, \beta \rangle\rangle = 0$ for all $\alpha \in \Omega^{k-1}(M)$ if and only if $\beta \in \mathcal{V}^k$. By Green's identity (62), the condition $\langle\langle d\alpha, \beta \rangle\rangle = 0$ for all α is equivalent to $\langle\langle \alpha, \delta\beta \rangle\rangle + \oint_{\partial M} (j^* \alpha) \wedge (j^* \star \beta) = 0$ for arbitrary α . The latter condition holds if and only if both $\delta\beta$ and $j^* \star \beta$ vanish, i.e. $\beta \in \mathcal{V}^k$. \square

E.2 Proof of Proposition 2

We first demonstrate (8b). Since d^+ (7) always first operates the orthogonal projection (6) onto $\text{im}(d)$, we have $\ker(d^+) \supset \text{im}(d)^\perp$. To show the final result of $\ker(d^+) = \text{im}(d)^\perp$, it suffices to check $\ker(d^+) \cap \text{im}(d) = \{0\}$. Suppose $\beta \in \ker(d^+) \cap \text{im}(d)$. The condition $\beta \in \text{im}(d)$ asserts that the preimage $d^{-1}(\{\beta\})$ is non-empty. The condition $\beta \in \ker(d^+)$ says that $0 \in d^{-1}(\{\beta\})$. In particular we must have $\beta = d0 = 0$. This completes the proof for (8b).

Next we show (8a). Eq. (7) implies that each element in $\text{im}(d^+)$ is an orthogonal projection of the origin onto an affine subspace (preimage $d^{-1}(\{P_{\text{im}(d)}\beta\})$) that is parallel to $\ker(d)$. Therefore $\text{im}(d^+) \subset \ker(d)^\perp$. On the other hand, every element $\alpha_0 \in \ker(d)^\perp$ is the minimizer of $\min_{d\alpha=d\alpha_0} \frac{1}{2} \|\alpha\|^2 \equiv \min_{\alpha-\alpha_0 \in \ker(d)} \frac{1}{2} (\|\alpha_0\|^2 + \|\alpha - \alpha_0\|^2)$. That is, $\alpha_0 = d^+(d\alpha_0)$, and hence $\alpha_0 \in \text{im}(d^+)$. Therefore $\text{im}(d^+) = \ker(d)^\perp$. This completes the proof for (8a).

The splittings (8) imply that d, d^+ are isomorphisms between the subspaces $\text{im}(d^+)$ and $\text{im}(d)$. Moreover, when being restricted to $\text{im}(d^+), \text{im}(d)$, they are the inverse of each other by construction. These properties imply (9) and Proposition 3. \square

E.3 Proof of Proposition 3

See Appendix E.2. \square

E.4 Proof of Proposition 4

To characterize the general form of elements in $\text{im}(d^+)$, we study $\alpha_0 = d^+ \beta$ for a general $\beta \in \Omega^{k+1}(M)$. By Proposition 3 we may assume $\beta \in \text{im}(d)$ ($P_{\text{im}(d)} \beta = \beta$) without loss of generality. By (7), α_0 is the solution for the problem of searching for an α that minimizes $\|\alpha\|^2/2$ subject to $d\alpha = \beta$. Taking a variation $\alpha_0 + \epsilon \dot{\alpha}$ of the constrained optimization at the optimizer $\alpha = \alpha_0$ yields

$$\langle\langle \alpha_0, \dot{\alpha} \rangle\rangle - \langle\langle d\dot{\alpha}, \psi \rangle\rangle = 0 \quad \text{for all } \dot{\alpha} \in \Omega^k(M) \quad (89)$$

for some Lagrange multiplier $\psi \in \Omega^{k+1}(M)$. By Green's identity (62), eq. (89) becomes

$$\langle\langle \alpha_0 - \delta\psi, \dot{\alpha} \rangle\rangle - \oint_M (j^* \dot{\alpha}) \wedge (j^* \star \psi) = 0 \quad \text{for all } \dot{\alpha} \in \Omega^k(M), \quad (90)$$

which implies that both $\alpha_0 - \delta\psi = 0$ and $j^* \star \psi = 0$. In conclusion, each element $\alpha_0 = d^+ \beta \in \text{im}(d^+)$ takes the form of $\alpha_0 = \delta\psi$ for some ψ that satisfies the co-Dirichlet boundary condition. \square

E.5 Proof of Proposition 5

To show the coexactness of η , or equivalently the exactness of $\hat{\eta} := \star\eta$, it suffices to check that $\oint_C \hat{\eta} = 0$ for all closed curve $C \subset M$. If M is the complement of a few obstacles in a simply-connected domain, then every C is homologous to a boundary curve along which $\oint_C \hat{\eta} = 0$ using the no-through condition $j^* \star \eta$. \square

E.6 Proof of Proposition 6

Here, we check that for each fixed $\eta \in \mathcal{V}^1$ the linear functional $\text{FLUX}(\eta)(\cdot): Z_{n-1}(M, \partial M) \rightarrow \mathbb{R}, S \mapsto \int_S \star\eta$ as defined in (16), is well-defined over $H_{n-1}(M, \partial M)$. Let $S_1, S_2 \in Z_{n-1}(M, \partial M)$ be homologous relative cycles. That is, when S_1, S_2 are treated as absolute $(n-1)$ -chains, we have $S_2 = S_1 + \partial U + \Sigma$ for some $U \in C_n(M)$ and $\Sigma \in C_{n-1}(\partial M)$. Our goal is to show $\int_{S_1} \star\eta = \int_{S_2} \star\eta$. Using the conditions $d \star \eta = 0$ and $j^* \star \eta = 0$ given by $\eta \in \mathcal{V}^1$, and that Σ completely lies in ∂M , we find $\int_{S_2} \star\eta = \int_{S_1} \star\eta + \int_{\partial U} \star\eta + \int_{\Sigma} \star\eta = \int_{S_1} \star\eta + \int_U d \star \eta + \int_{\Sigma} j^* \star \eta = \int_{S_1} \star\eta$. \square

E.7 Proof of Proposition 7

Here, we show that $\ker(\text{FLUX}) = \text{im}(d^+)$. For notation convenience, we write $\hat{\eta} = \star\eta$ for each $\eta \in \mathcal{V}^1$ to absorb the Hodge star. Let us also call $\Omega_D^k(M) = \{\alpha \in \Omega^k(M) \mid j^* \alpha = 0\}$ the space of Dirichlet-condition-satisfying k -forms. Note that the Dirichlet de Rham complex $\cdots \xrightarrow{d} \Omega_D^k(M) \xrightarrow{d} \Omega_D^{k+1}(M) \xrightarrow{d} \cdots$ is the cochain complex that is dual to the relative chain complex $C^\bullet(M, \partial M)$ through the standard de Rham pairing $(A, \alpha) \mapsto \int_A \alpha$.

Now, each $\hat{\eta} = \star\eta, \eta \in \mathcal{V}^1$, is a general member $\hat{\eta} \in \Omega_D^{n-1}(M)$ satisfying $d\hat{\eta} = 0$. Our goal is to show that $\int_S \hat{\eta}$ for all relative cycles $S \in Z_{n-1}(M, \partial M)$ if and only if $\hat{\eta} = d\hat{\psi}$ for some $\hat{\psi} \in \Omega_D^{n-2}(M)$ (cf. Proposition 4).

One of the directions (" \Leftarrow ") in the equivalence statement only requires elementary calculus. Suppose $\hat{\eta} = d\hat{\psi}$ for some $\hat{\psi} \in \Omega_D^{n-2}(M)$, $j^* \hat{\psi} = 0$. We claim $\int_S \hat{\eta} = 0$ for all $S \in Z_{n-1}(M, \partial M)$. Note that these surfaces S has the property that ∂S is either empty or ∂S lies completely in ∂M . Thus $\int_S \hat{\eta} = \int_S d\hat{\psi} = \int_{\partial S} \hat{\psi} = \int_{\partial S} j^* \hat{\psi} = 0$.

Now let us show the other direction (" \Rightarrow ") using linear algebraic techniques. The statement we want to show is that if $\hat{\eta} \in \Omega_D^{n-1}(M)$ satisfies $\int_S \hat{\eta} = 0$ for all cycles $S \in Z_{n-1}(M, \partial M)$, then $\hat{\eta}$ is exact in the Dirichlet de Rham complex. To see this, inspect the following diagram in which ∂ and d are adjoint of each other

$$\begin{array}{ccc} C_{n-1}(M, \partial M) & \xrightarrow{\partial} & C_{n-2}(M, \partial M) \\ \uparrow \text{dual space} & & \uparrow \text{dual space} \\ \hat{\eta} \in \Omega_D^{n-1}(M) & \xleftarrow{d} & \Omega_D^{n-2}(M). \end{array} \quad (91)$$

By the Theorem of Four Fundamental Subspaces in linear algebra, we have that $\text{im}(d) \subset \Omega_D^{n-1}$ equals to the *annihilator* of $\ker(\partial) \subset C_{n-1}(M, \partial M)$. The condition $\int_S \hat{\eta} = 0$ for all $S \in \ker(\partial)$

in $C_{n-1}(M, \partial M)$ ensures that $\hat{\eta}$ is in the annihilator of $\ker(\partial)$, and therefore $\hat{\eta}$ is exact. \square

E.8 Proof of Proposition 8

To show that the FLUX: $\mathcal{V}^1(M) \rightarrow H_{n-1}(M, \partial M)^*$ is surjective, it suffices to take a generator basis (S_1, \dots, S_m) for $H_{n-1}(M, \partial M)$ and for each $j = 1, \dots, m$ construct a harmonic field $\zeta^j \in \mathcal{H}_C^1(M)$ such that $\int_{S_i} \zeta^j = \delta_i^j$. This construction is described in Section 3.4.1 and verified by Proposition 9. \square

E.9 Proof of Proposition 9

Our first goal is to show $\int_M \zeta^i \wedge \xi_j = \delta_j^i$. Let us call $\hat{\xi}_j := \star^{-1} \xi_j = (1 - dd^+) \delta_{S_j} \in \mathcal{H}_C^1(M)$. Note that $\int_M d^+(\cdot) \wedge \star \hat{\xi}_j = 0$ by the orthogonality between $\text{im}(d^+)$ and co-Dirichlet harmonic 1-forms. Now,

$$\begin{aligned} \int_M \zeta^i \wedge \xi_j &= \int_M \zeta^i \wedge \star \hat{\xi}_j = \int_M (1 - dd^+) (\star \delta_{C_i}) \wedge \star \hat{\xi}_j \\ &= \int_M (\star \delta_{C_i}) \wedge \star \hat{\xi}_j. \end{aligned} \quad (92)$$

By substituting $\hat{\xi}_j = (1 - dd^+) \delta_{S_j}$ and Appendix A.1.7, we obtain

$$\int_M \zeta^i \wedge \xi_j = \int_M (\star \delta_{C_i}) \wedge \star \hat{\xi}_j \quad (93)$$

$$= \int_M (\star \delta_{C_i}) \wedge \star \left((1 - dd^+) \delta_{S_j} \right) \quad (94)$$

$$= \int_M \delta_{C_i} \wedge (1 - dd^+) \delta_{S_j} \quad (95)$$

$$= \int_M \underbrace{\delta_{C_i} \wedge \delta_{S_j}}_{=\delta_{C_i \cap S_j}} + \underbrace{(-1)^n \int_{C_i} dd^+ \delta_{S_j}}_{=0 \text{ since } \partial C_i = 0} \quad (96)$$

$$= [C_i \cap S_j] = \delta_{ij}. \quad (97)$$

This dual basis property $\int_M \zeta^i \wedge \xi_j = \delta_j^i$ also ensures that the coefficients c_j in (28) are given by $c_j = \int_M \eta \wedge \xi_j$. What is left to show is that $\int_M \eta \wedge \xi_j = \text{FLUX}(\eta)(S_j)$:

$$\int_M \eta \wedge \xi_j = \int_M \eta \wedge \star \left((1 - dd^+) \delta_{S_j} \right) \quad (98)$$

$$= \int_M \delta_{S_j} \wedge \star \eta = \int_{S_j} \star \eta = \text{FLUX}(\eta)(S_j), \quad (99)$$

where we have used $\eta \perp \text{im}(d)$ (Proposition 1). \square